NASA Tech Briefs

National Aeronautics and
Space Administration

Electronic Components and Circuits

Electronic Systems

Physical Sciences

Materials

Computer Programs

Mechanics

Machinery

Fabrication Technology

Mathematics and Information Sciences

Life Sciences

98-06

June 1998

INTRODUCTION

Tech Briefs are short announcements of new technology derived from the research and development activities of the National Aeronautics and Space Administration. These Briefs emphasize information considered likely to be transferable across industrial, regional, or disciplinary lines and are issued to encourage commercial application.

Availability of NASA Tech Briefs and TSP's

Distribution of NASA Tech Briefs, a monthly periodical publication, is limited to engineers in U.S. Industry and to other domestic technology transfer agents. Requests for individual Tech Briefs or for Technical Support Packages (TSP's) announced herein should be addressed to

NASA Center for AeroSpace Information
Technology Transfer Office
800 Elkridge Landing Rd.
Linthicum Heights, MD 21090-2934
Telephone No. (301) 621-0245

Please reference the three-letter, five-digit control number located at the end of each Tech Brief. Information on NASA's Technology Utilization Program, its documents, and services is also available at the same facility.

Technology Utilization Officers and Patent Counsels are located at NASA field installations to provide technology-transfer access to industrial users. Inquiries can be made by writing to NASA field installations listed below.

Technology Utilization Officers and Patent Counsels

Ames Research Center
Technology Utilization Officer
Mail Code 223-3
Moffett Field, CA 94035

Patent Counsel
Mail Code 200-11
Moffett Field, CA 94035

Goddard Space Flight Center
Technology Utilization Officer
Mail Code 702-1
Greenbelt, MD 20771

Patent Counsel
Mail Code 204
Greenbelt, MD 20771

Lyndon B. Johnson Space Center
Technology Utilization Officer
Mail Code IC-4
Houston, TX 77058

Patent Counsel
Mail Code AL3
Houston, TX 77058

John F. Kennedy Space Center
Technology Utilization Officer
Mail Stop PT-PMO-A
Kennedy Space Center, FL 32899

Patent Counsel
Mail Code PT-PAT
Kennedy Space Center, FL 32899

Langley Research Center
Technology Utilization Officer
Mail Stop 143
Hampton, VA 23665

Patent Counsel
Mail Code 279
Hampton, VA 23665

Lewis Research Center
Technology Utilization Officer
Mail Stop 7-3
21000 Brookpark Road
Cleveland, OH 44135

Patent Counsel
Mail Code LE-LAW
21000 Brookpark Road
Cleveland, OH 44135

Jet Propulsion Laboratory
Technology Utilization Officer
Mail Stop 156-211
4800 Oak Grove Drive
Pasadena, CA 91109

NASA Resident Office-JPL
Technology Utilization Officer
Mail Stop 180-801
4800 Oak Grove Drive
Pasadena, CA 91109

Patent Counsel
Mail Code 180-801
4800 Oak Grove Drive
Pasadena, CA 91109

George C. Marshall Space Flight Center
Technology Utilization Officer
Code AT01
Marshall Space Flight Center, AL 35812

Patent Counsel
Mail Code CC01
Marshall Space Flight Center, AL 35812

John C. Stennis Space Center
Technology Utilization Officer
Code HA-30
Stennis Space Center, MS 39529

NASA Headquarters
Technology Utilization Officer
Code CU
Washington, DC 20546

Assistant General Counsel for Patent Matters
Code GP
Washington, DC 20546

Dryden Flight Research Center
Technology Utilization Officer
M/S D21-31
Bldg. 4832 Whse 7
Lilly Dr.
Edwards, CA 93523

BLANK PAGE

NASA TechBriefs

National Aeronautics and
Space Administration

June 1998
98-06

BLANK PAGE

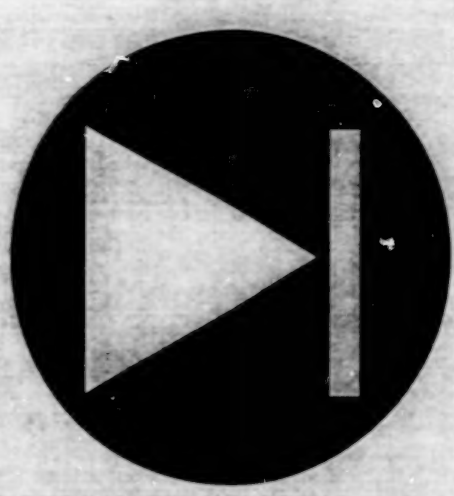

Electronic Components and Circuits

Hardware, Techniques, and Processes

Books and Reports

BLANK PAGE

DC-Excited Thermostrain-Gauge Signal-Conditioning Circuit

Gauge-resistance and temperature signals are separated.

Dryden Flight Research Center, Edwards, California

The figure illustrates a dc-excited Anderson-loop circuit that includes (1) thermocouples for measuring the temperature of the strain gauge and (2) a signal-conditioning circuit that separates the temperature and strain-gauge signals in the sense that one output voltage is proportional to the change in the strain-gauge resistance and another voltage is proportional to the thermoelectric voltage indicative of the temperature of the strain gauge.

The concept of the Anderson loop was discussed previously in two articles in *NASA Tech Briefs*; namely, "The Anderson Current Loop" (DRC-00001), *NASA Tech Briefs*, Vol. 18, No. 12, (December 1994), page 30; and "Patent Statement on the Anderson Current Loop" (ARC-13376), Vol. 20, No. 11, (November 1996), page 12a. To recapitulate: In the basic Anderson current loop, voltage drops in lead wires are excluded from measurement by use of the well-known Kelvin technique, in which a known current is supplied via two lead wires to a resistance to be determined, the voltage across this resistance is coupled to a high-input-resistance voltmeter via two other lead wires, and the voltage drops in these voltage-measurement lead wires can be neglected because they carry negligible current by virtue of the high input resistance of the voltmeter.

Here, a known constant current I is supplied to a strain gauge of resistance $R + \Delta R$, (where R is an initial value and ΔR is a change caused by the combined effects of strain and temperature). The strain-gauge resistance is connected in series with two thermocouple wires of resistance R_{w1} and R_{w2}, respectively. These wires are both made of the same one of two thermocouple alloys and are of the same length, so that $R_{w1} = R_{w2}$. Two other wires (R_{w3} and R_{w4}) made of the other thermocouple alloy, are connected to the terminals for measuring the voltage drop in the strain-gauge resistance. A reference resistor ($R_{ref} = R$) at a reference or ambient temperature is also connected in series with the strain-gauge resistance.

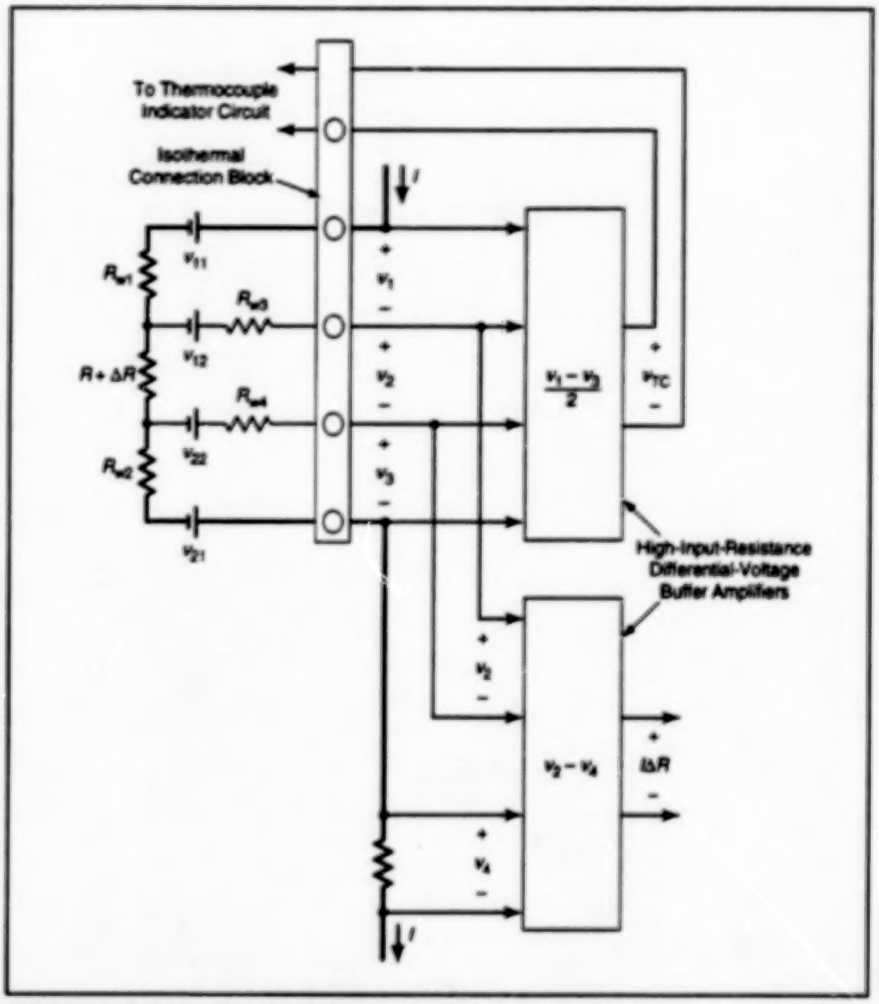

Differences Between Terminal Voltages provide indications of the temperature of the strain gauge and the change in the strain-gauge resistance.

The thermoelectric voltage of thermocouple (R_{w1},R_{w3}) is given by

$$v_{TC1} = v_{11} - v_{12};$$

the thermoelectric voltage of thermocouple (R_{w2},R_{w4}) is given by

$$v_{TC2} = v_{21} - v_{22}.$$

The thermoelectric-output-voltage level of each thermocouple represents the temperature of its connection to the strain gauge.

Straightforward algebraic manipulation of the equations that relate the terminal voltages v_1 through v_4 with the voltage drops in the various resistances and with the thermoelectric voltages yields the following equations for the desired output voltages:

$$v_{TC} = (v_1 - v_3)/2 \text{ and}$$
$$I\Delta R = (v_2 - v_4).$$

As indicated in the figure, the terminal voltages v_1 through v_4 are coupled to Anderson subtractors comprised of buffered differential level shifting amplifiers wired to implement these equations. The subtractor outputs are then the output thermoelectric voltage v_{TC} and resistance-change voltage $I\Delta R$.

This work was done by Karl F. Anderson of Analytical Services and Materials for **Dryden Flight Research Center**. *Further information is contained in a TSP [see page 1].*

DRC-96-10

Micromachined Interferometric Optoelectronic Display Devices

Miniature Fabry-Perot interferometers would be used as modulators to mix colors.

NASA's Jet Propulsion Laboratory, Pasadena, California

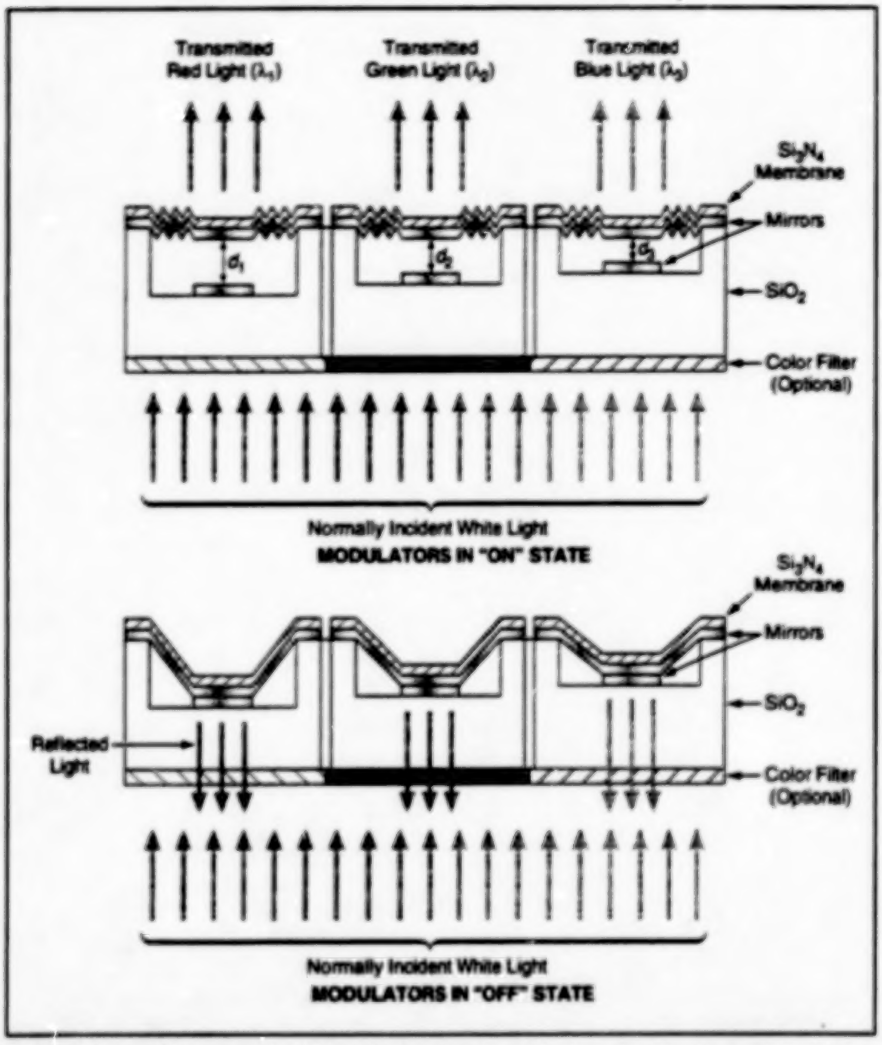

Each of Three Micromachined Interferometers in a pixel would either transmit light at a resonant wavelength λ_i when relaxed at gap d_i, or else would not transmit when its mirrors were pulled together by voltage applied to electrostatic-deflection electrodes.

Devices containing planar arrays of micromachined, electrostatically adjustable Fabry-Perot interferometers are undergoing development. These devices could be designed, for example, as color high-definition television displays, as larger flat-panel displays for indoor and outdoor entertainment and advertising, as filter arrays for spectroscopy, and as modulator arrays for optical computing and switching. In comparison with state-of-the-art flat-panel display devices based on liquid crystals, plasmas, and electroluminescence, the present devices offer potential advantages of high speed, insensitivity to changes in temperature, low power consumption, wide viewing angle, scalability, light weight, and long life.

A related concept of using two-stage, micromachined, electrostatically adjustable Fabry-Perot interferometers as rapidly tunable color filters and shutters was presented in "Micromachined Opto/Electro/Mechanical Systems" (NPO-19467), *NASA Tech Briefs*, Vol. 21 , No. 3 (March 1997), page 50, and "Micromachined Tunable Optical Interference Filters" (NPO-19456), *NASA Tech Briefs*, Vol. 21 , No. 3 (March 1997), page 111. The devices being developed according to the present concept are based on the same physical principles but differ in significant details of design and modes of operation.

In a three-color television display device according to the present concept, each pixel would contain three micromachined, electrostatically adjustable Fabry-Perot interferometers, each serving as a modulator for light of one of three wavelengths (see figure). Each micromachined interferometer would contain two parallel, flat, partially transparent mirrors — one on a springy silicon nitride membrane and the other on a stationary glass substrate. The mirrors and the gap between them would constitute an optical cavity with resonant transmission peaks at wavelengths equal to integer submultiples of twice the size of the gap; that is, the interferometer would transmit most of the light at these wavelengths and reflect most of the light at other wavelengths.

The nominal size of the gap in each micromachined interferometer would be selected so that its resonant wavelength in the visible part of the spectrum was that of the desired color. The display panel would be illuminated with white light from its back side (the lower side in the figure). Optionally, color filters could be formed on the back side registered with the corresponding interferometers to provide additional selectivity for greater purity of the colors.

When voltage was not applied to the electrostatic-deflection electrodes, the springy silicon nitride membrane in each interferometer would maintain the nominal gap and therefore light of the nominal wavelength would pass through to the front (top in the figure) side, where it would be seen. When voltage was applied to the electrostatic-deflection electrodes of a given color interferometer in a given pixel, the spring force would be overcome and the two mirrors drawn together; this would eliminate the resonant gap, causing the two mirrors to act as ordinary mirrors so that light would not pass through to the front. The net effect would be that each interferometer would act as a light valve or modulator for its assigned color. Thus, by opening each light valve for a specified fraction of each image-repetition cycle, one could mix specified proportions of each color. Since the viewer's eye could not spatially resolve the individual interferometers or temporally resolve the individual flashes of light, the viewer would get the impression of a desired composite color emanating from the pixel.

This work was done by Tony K. T. Tang, Linda M. Miller, Michael H. Hecht, and Judith A. Podosek of Caltech for **NASA's Jet Propulsion Laboratory**. *Further information is contained in a TSP [see page 1].*

NPO-19527

Column-Loading Input Chip for Neural-Network Module

All functions would be performed within a cycle time of 250 ns.

NASA's Jet Propulsion Laboratory, Pasadena, California

The column-loading input chip (CLIC) is a conceptual integrated-circuit chip that would serve as an interface between (1) any of various sources of image data and (2) a three-dimensional analog neural network (3DANN) of the type described in "Neural-Network Modules for High-Speed Image Processing" (NPO-19881), *NASA Tech Briefs*, Vol. 21, No. 10 (October 1997), page 26. The overall functions of the CLIC (see Figure 1) would be to load 8-bit digital image-intensity signals from a 64 × 64 array of pixels, convert these digital signals to an array of 64 × 64 analog voltages, and couple these voltages simultaneously to all of the corresponding 64 × 64 input terminals of the 3DANN. To prevent a data-input bottleneck, the CLIC is designed to perform these functions within a 3DANN-cycle time of 250 ns. The digital-to-analog conversion would be accomplished in only about 140 ns, leaving about 110 ns for processing by the 3DANN. The CLIC is also designed to satisfy requirements of compactness and low power consumption.

As part of the design to achieve the required high speed, the digital-to-analog conversion would be performed locally for each of the 64 × 64 inputs to the 3DANN, by use of a 64 × 64 array of multiplying digital-to-analog converters (MDACs) at the corresponding locations. The input digital image-intensity signals for the MDACs would be coupled to the MDACs in pipeline fashion, by use of row and column arrays of 8-byte shift registers (see Figure 2).

The data would be shifted into the CLIC in parallel 8 bytes corresponding to rows or columns of pixels in the source image. It would be necessary to accommodate input in row or column groups of pixels in order to enable changes in direction of rastering when a 64 × 64 array of pixels reached the edge of a larger image of which it was a part.

For input in columns, the data would be shifted in rightward from the left edge; for input in rows, the data would be shifted in downward from the top edge or upward from the bottom edge. As the data for each successive column or row of new data was shifted in, the data already in each of the shift registers in the interior of the array would be shifted rightward (for input by columns) or up or down (for input by rows), and the data in the registers in the rightmost column (in the case of column input) or in the bottom or top row (in the case of row input) would be destroyed and replaced by new data.

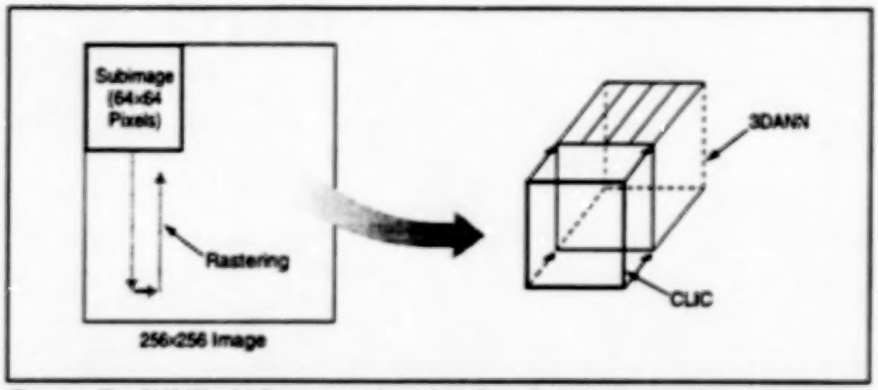

Figure 1. **The CLIC Would Serve as an Input Interface**, for example, to perform rastering on a sequence of digitized 64 × 64-pixel subimages from 256 × 256-pixel image source and digital-to-analog conversion for input to a 64 × 64-pixel 3DANN.

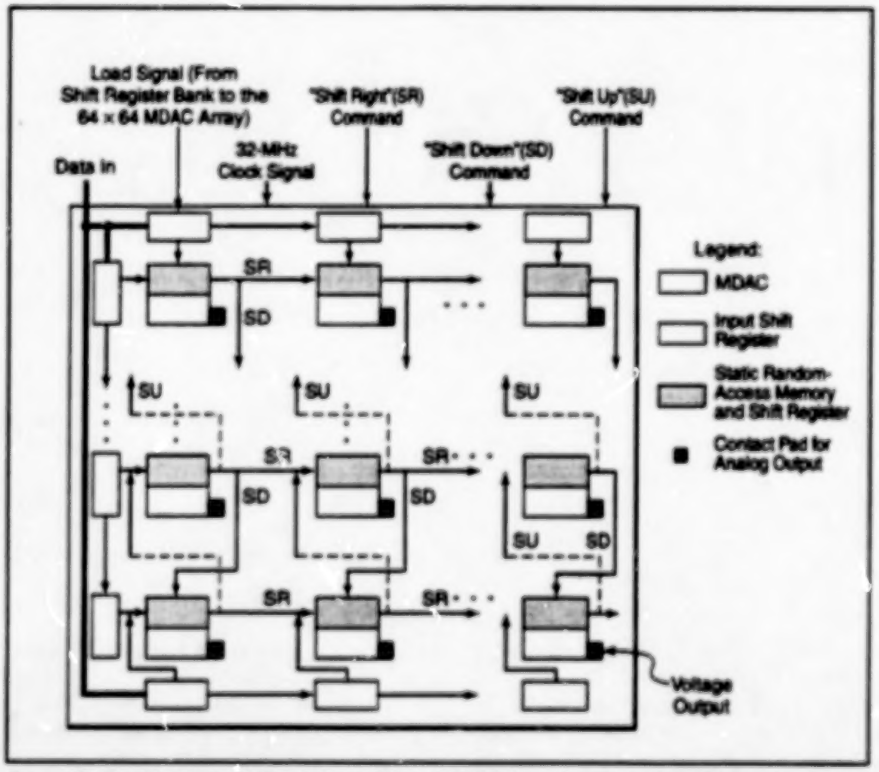

Figure 2. **The CLIC Would Contain an Array of MDACs and shift registers.** Digital signals at a basic clock rate of 32 MHz would command the shift registers to shift rightward, upward, or downward, and would control the MDACs. The input shift registers would be arranged in banks with eight-byte parallel input and output, so that all the input data for a full column of 64 × 64 array could be loaded in eight clock cycles.

While the data were being shifted into the CLIC, the MDACs would continue to operate on the data from the preceding 3DANN cycle. When all the data for a 64 × 64 array of pixels had been shifted in, all MDACs would simultaneously perform analog-to-digital conversions on the current contents of their local shift registers. After a settling time of about 140 ns, the analog output voltages of the MDACs would be ready for processing by the 3DANN. During the remaining 110 ns of the cycle, these voltages would continue to be available to the 3DANN for processing, and image data for the next cycle would be shifted in.

This work was done by Tuan A. Duong of Caltech for **NASA's Jet Propulsion**

Laboratory. *Further information is contained in a TSP [see page 1].*

In accordance with Public Law 96-517, the contractor has elected to retain title to this invention. Inquiries concerning rights for its commercial use should be addressed to

Technology Reporting Office
JPL
Mail Stop 122-116
4800 Oak Grove Drive
Pasadena, CA 91109
(818) 354-2240

Refer to NPO-20033, volume and number of this NASA Tech Briefs issue, and the page number.

Lightweight, Radiation-Resistant EMI Shields

Effective shielding can be achieved at fractions of the weights of aluminum boxes.

Lewis Research Center, Cleveland, Ohio

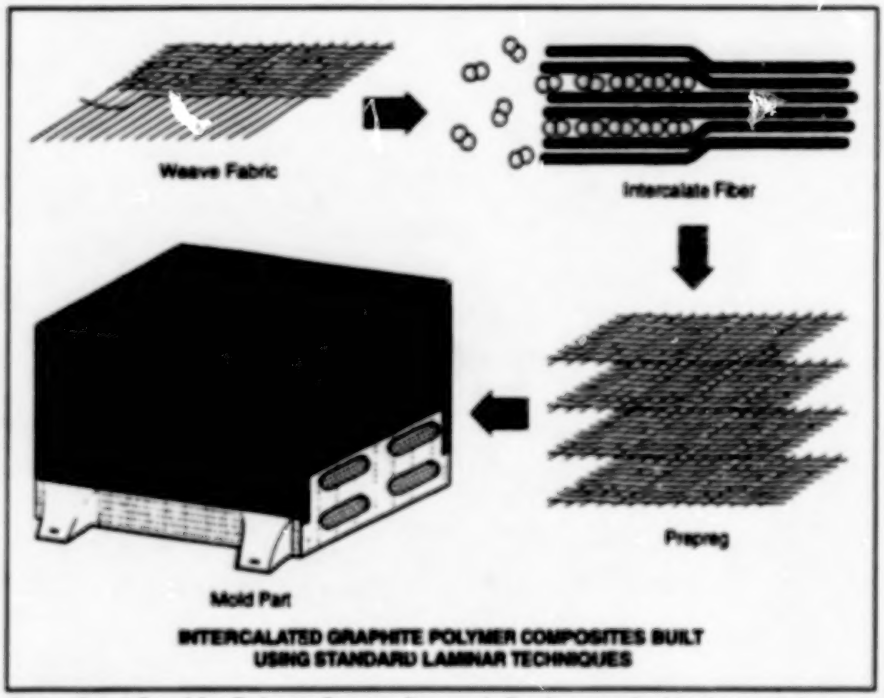

Intercalated Graphite Polymer Composites are built using standard laminar techniques.

Due to their low density and exceptionally high strength and modulus, graphite fiber composites are being used increasingly for the fabrication of aircraft and spacecraft. Because of their superior mechanical properties, these composites have been replacing metals, such as aluminum alloys, in many applications. The replacement of metals has been slow, however, when high electrical conductivity is needed because of the relatively poor electrical conductivity (< 0.1 percent of metals) of composite materials. Designers have also shied away from graphite-polymer composites in applications where shielding from ionizing radiation is important, because of the poor performance of these composites.

These shortcomings of graphite-fiber polymer composites can be addressed by intercalating the fibers before fabricating the composites. Intercalation is the insertion of guest atoms or molecules (intercalates) in between the carbon layers of the fibers. If the intercalate is chosen carefully, the electrical conductivity of the composite can be increased nearly an order of magnitude, and the specific radiation shielding can surpass low density metals.

Two intercalates, bromine and iodine monobromide, have been shown to have the right combination of properties to make them commercially viable options. They combine the virtues of high electrical conductivity, high thermal conductivity, and good radiation shielding with excellent stability and easy processibility.

Bromine has been shown to intercalate a wide variety of pitch-based and vapor-grown graphite fibers. Most of the research has centered around Amoco's Thornal fibers. Bromine has been shown to enhance the conductivity of P-55, P-75, PO-100, P-120, and K-1100 fibers by a factor of three to six. The resulting material has an electrical conductivity surpassing that of stainless steel. Furthermore, these intercalation compounds are stable to temperature well above the processing temperature for most resins, and are impervious to moisture and ultra-high vacuum. Fabrication of composites from intercalated fibers does not degrade their properties, and composite properties can be predicted by using a simple rule-of-mixture. Although intercalation does not enhance either the mechanical properties or the thermal conductivity of graphite fiber composites, neither does it degrade them. The mechanical properties are virtually identical with those of pristine fibers, except that there is an enhancement in the interlaminar shear properties. The thermal conductivities of these fibers are among the highest of all materials, exceeding such metals as aluminum and copper. Also, because of the high thermal absorption and emissivity of graphite fibers, radiant heat is rejected much more efficiently from electrical components than when they are encased in highly reflective metals. The mass absorption coefficient for ionizing radiation by composites made from intercalated fibers is enhanced by a factor of four, to a value exceeding that of aluminum.

Iodine monobromide has not been studied as extensively as bromine has as an intercalate for graphite fibers. Those studies that have been done reveal intercalation compounds nearly identical with those utilizing bromine. The exception is in the mass absorption coefficient for ionizing radiation, which is nearly twice that of bromine intercalation compounds, and three times that of aluminum. The implication is that iodine monobromide intercalated fiber composites can provide radiation shielding equal to that of aluminum with one-third the mass.

The primary application envisioned for this technology is electromagnetic interference (EMI) shielding of electronics. Calculations indicate that the shielding effectiveness of these composites, while not as high as that of aluminum, is higher than the requirements for many applications, and higher than that of joints and penetrations through metallic boxes. Experimental studies confirm the high

shielding effectiveness calculations. The surface conductivity, while not as high as that of metals, is high enough that no special surface treatments (sanding off the surface polymer layer, etc.) are required. These materials can be used effectively with conventional EMI shielding gasketing strategies.

The total achievable mass savings depends on the particular requirements of the shield. If the limiting factor is shielding from high-energy radiation, a mass savings of 66 percent is achievable. If the limit is strength, 86 percent of the mass can be saved. Finally, if the limit is stiffness (modulus), over 90 percent of the mass can be saved. The implications for such weight savings can be dramatic. In spacecraft, because the payload is a smaller portion of the spacecraft than the power and communications systems, the payload may be increased by as much as 40 percent. In communications satellites, the mass savings could be taken up in attitude-control fuel, extending the useful lifetime of the spacecraft. In some cases, it could enable the launch by smaller and cheaper launch vehicles. In aircraft, decreased weight would allow for fuel savings, which, when figured over the life of the aircraft, could be substantial. For consumer products, such as notebook computers and cellular telephones, lower weight itself might be a significant selling point.

This work was done by James R. Gaier of **Lewis Research Center**. *Further information is contained in a TSP [see page 1].*

Inquiries concerning rights for the commercial use of this invention should be addressed to NASA Lewis Research Center, Commercial Technology Office, Attn: Tech Brief Patent Status, Mail Stop 7–3, 21000 Brookpark Road, Cleveland, Ohio 44135. Refer to LEW-16535.

Variable-Wavelength Micromachined Fabry-Perot Interferometers

Displayed colors would be varied at will.

NASA's Jet Propulsion Laboratory, Pasadena, California

The figure schematically shows a micromachined Fabry-Perot interferometer that, when fully developed, would be part of a two-dimensional array of such interferometers in a flat-panel display device. The interferometers, arrays, and display devices according to this concept would be similar to those described in "Micromachined Interferometric Optoelectronic Display Devices" (NPO-19527), page 8. The basic principles of design and operation are the same, but there would be differences in some of the details.

The major difference in design would be that a device of this type would contain only one micromachined Fabry-Perot interferometer per pixel instead of three as in the devices of the preceding article. The major difference in operation is that instead of using each micromachined Fabry-Perot interferometer as an on/off modulator for light of a preset wavelength, one would use each such interferometer as a tunable band-pass filter and "off" switch: the voltage applied to the electrostatic-deflection electrodes of the interferometer in each pixel could be varied as a function of time to make light of a chosen wavelength pass through at a given time, or the voltage could be increased to a level sufficient to draw the interferometer mirrors together so that no light would pass through. That is, by controlling the voltage applied to each pixel, one could either make it appear to glow in a chosen color or else go dark.

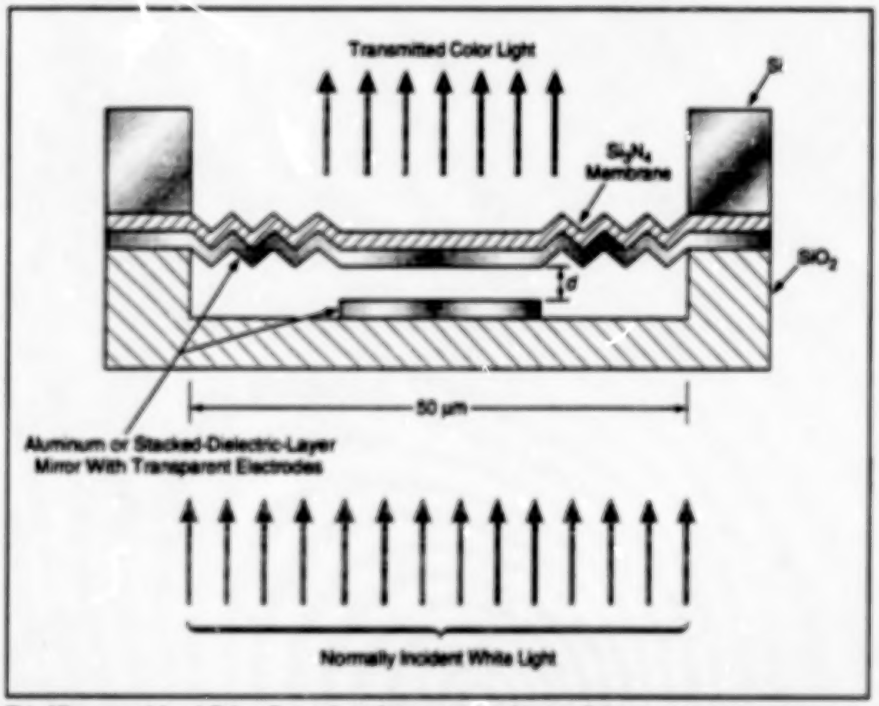

This Micromachined Fabry-Perot Interferometer would pass light at a resonant wavelength equal to $2nd/m$, where n is the index of refraction of the medium between the mirrors, d is the gap width shown in the figure, and m is an integer that denotes the order of interference. The voltage applied to the transparent electrodes would be varied to vary d and thus the transmitted color.

The feasibility of this concept was demonstrated in an experiment on a prototype. The distance between the mirrors was varied, causing the transmitted color to vary between red and blue.

This work was done by Tony K. T. Tang, Linda M. Miller, and Judith A. Podosek of Caltech for **NASA's Jet Propulsion Laboratory**. *Further information is contained in a TSP [see page 1].*

NPO-19528

Instrument Records Electric Fields Generated by Lightning

This instrument complements another instrument that measures magnetic fields generated by lightning.

John F. Kennedy Space Center, Florida

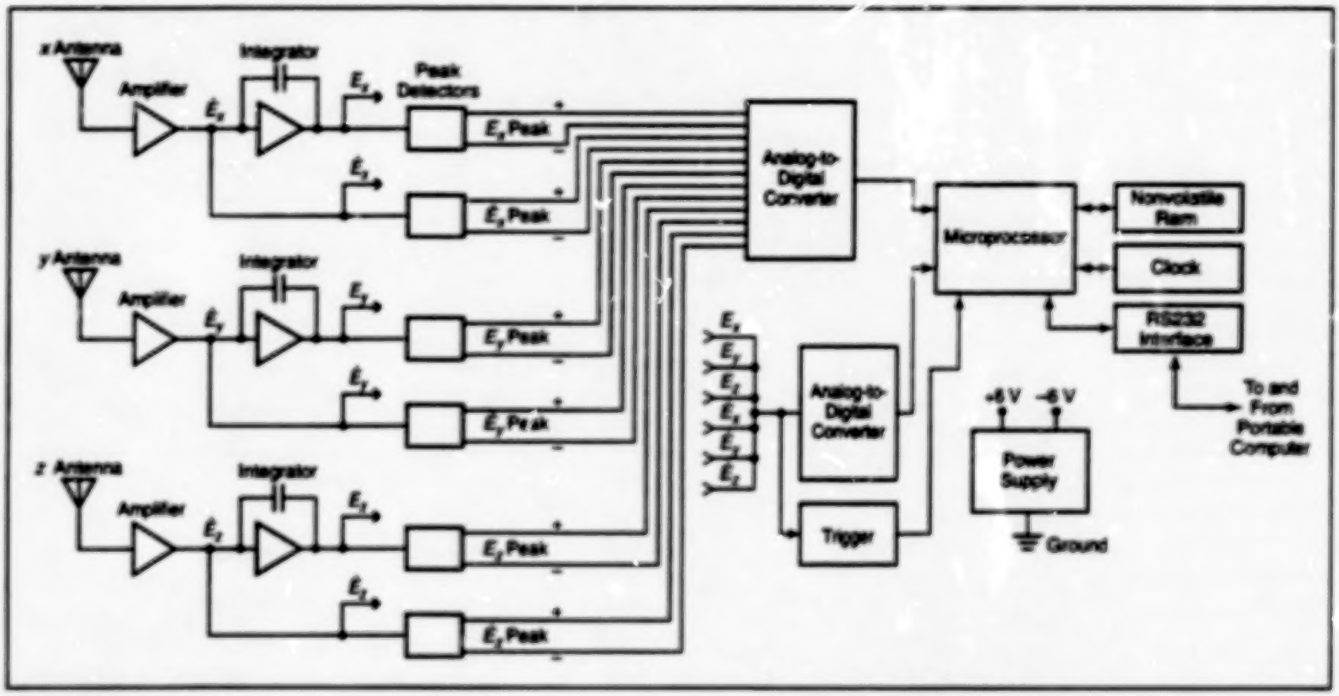

Three Orthogonal Antennas sense the three orthogonal components of the rate of change of electric field; that is, $\dot{E}_x$, $\dot{E}_y$, and $\dot{E}_z$. These components and their time integrals (proportional to the electric field) are sampled and recorded for subsequent analysis.

A portable, self-contained, compact instrument measures and records transient electric fields generated by nearby lightning strikes. This instrument complements, and in many respects is similar to, the one described in "Instrument Records Magnetic Fields Generated by Lightning" (KSC-11769), *NASA Tech Briefs*, Vol. 19, No. 4 (April 1995), page 38. Both instruments are designed to be placed near sensitive electronic equipment before thunderstorms begin. The data recorded by the instruments during thunderstorms can be analyzed afterward to determine whether the electromagnetic fields associated with the lightning were strong enough that they might have damaged and/or affected the operation of the sensitive equipment. Thus, the instruments provide data that can be used in deciding whether the sensitive equipment should be tested for damage and/or other effects caused by lightning. Typical installations in which the instruments could prove beneficial include outdoor sensing equipment, computer rooms, broadcasting stations, and powerplant-control rooms.

The present instrument (see figure) includes three orthogonal antennas on an electrically conductive sphere. Each antenna senses one of the three orthogonal components of the transient electric field. The current $i(t)$ induced in each antenna is proportional to the rate of change of the electric-field component $E(t)$, and is given by

$$i(t) = kA\varepsilon \frac{\partial E}{\partial t}$$

where t is time, A is the area of the antenna, ε is the permittivity of air (very close to ε_0, the permittivity of the vacuum), and k is a constant that expresses the concentration of the electric field in the vicinity of the antenna or a similar electrically conductive object. The spherical shape was chosen because k for a sphere is easily determined and is found to equal 3.

In the instrument, the currents are measured to determine the rates of change of the components of the electric field. The current signals are also integrated to obtain signals proportional to the electric-field components.

The instrument includes a microprocessor that controls its overall operation. It also includes an analog-to-digital converter and a sampling clock. Under control by the microprocessor, the analog-to-digital converter samples the waveform of one component of the electric field at a rate of 10 MHz for a duration of 50 μs. (The reason for not sampling all three waveform components is simply that doing so would consume too much power.) Also under control by the microprocessor, the peak values of all three components of the electric field and their time derivatives are sampled and compared with specified threshold levels during intervals of 1 ms. The electric-field waveform sample values and their times are stored in a nonvolatile random-access memory (NVRAM). The peak electric-field and derivative sample values that exceed the threshold levels, and their times, are also stored in the NVRAM.

The stored values are subsequently read out by use of a portable computer. The instrument is powered by batteries and can operate unattended for as long as two weeks. The inclusion of the NVRAM prevents the loss of data in the event of a power failure. The batteries can be changed in the field, so that the instrument can remain in place and continue to measure the electric field without interruption.

With their 10-MHz sampling rate, both this instrument and the previously reported magnetic-field instrument measure electromagnetic fields generated by lightning more accurately than do portable commercial magnetic-field meters. Lightning waveforms typically include frequencies

up to tens of megahertz, while the commercial meters, which are designed to measure magnetic fields of high-voltage power lines, are usually limited in frequency response to a few hundred hertz.

This work was done by Pedro J. Medelius and Howard James Simpson formerly of I-Net for **Kennedy Space Center**.

Further information is contained in a TSP [see page 1].
KSC-11953

Books and Reports

Micromachined Tunneling Accelerometer for Use in Outer Space

Two short reports describe a micromachined quantum-mechanical-tunneling accelerometer and radiation-hardened support electronics designed for use in outer space. Like the micromachined tunneling accelerometers described previously in *NASA Tech Briefs*, this device is based on the use of electronic sensing/feedback control circuitry that measures acceleration in terms of an electrostatic-deflection voltage necessary to maintain a small constant distance (typically a few Angstroms) between a membrane and a tunneling tip in a mechanical acceleration-sensing/electron-tunneling device. This accelerometer is implemented in a multichip integrated-circuit module designed to function at temperatures from −40 to +70 °C in a 100-krad (Si) radiation environment. The accelerometer was tested in operation during exposure to a total dose of 100 krad (Si) of γ radiation with from a ^{60}Co source; the tunneling action was not affected by the radiation. The device is to be flown aboard the Space Technology Research Vehicle-2 spacecraft.

This work was done by Vardges Victor Boyadzhyan-Sevak of Caltech for **NASA's Jet Propulsion Laboratory**. *To obtain copies of the reports, "ATC ELECTRON TUNNELING ACCELEROMETER INTEGRATED SENSOR CIRCUITRY FOR SPACE APPLICATIONS" and "Tunneling Accelerometer MULTICHIP MODULE (Integrated Sensor) THIN FILM TECHNOLOGY RADIATION HARDENED MCM, see TSP's [page 1].*

In accordance with Public Law 96-517, the contractor has elected to retain title to this invention. Inquiries concerning rights for its commercial use should be addressed to

Technology Reporting Office
JPL
Mail Stop 122-116
4800 Oak Grove Drive
Pasadena, CA 91109
(818) 354-2240

Refer to NPO-20013, volume and number of this NASA Tech Briefs *issue, and the page number.*

BLANK PAGE

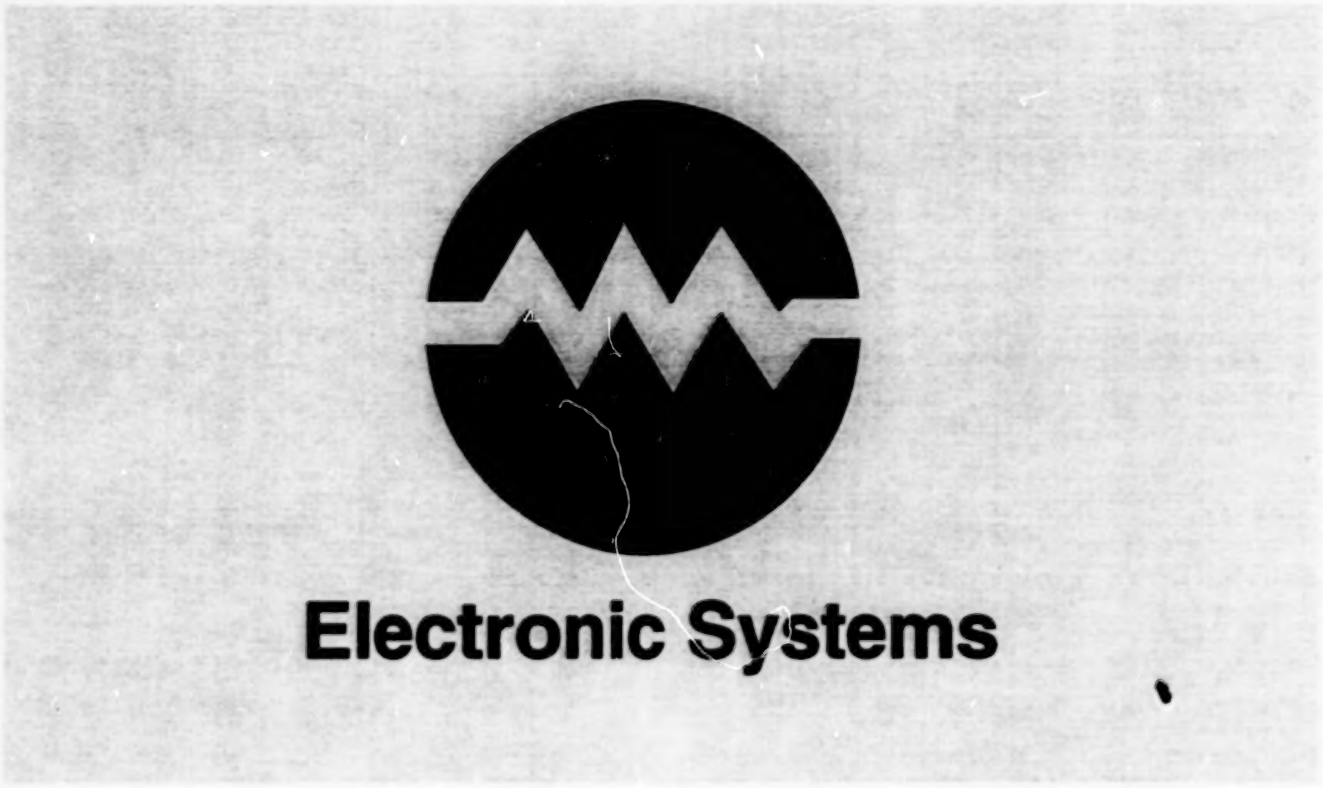

Hardware, Techniques, and Processes

Books and Reports

BLANK PAGE

Optoelectronic System Measures Tile Cavities

Three-dimensional measurement of a cavity is accomplished in less than one second.

John F. Kennedy Space Center, Florida

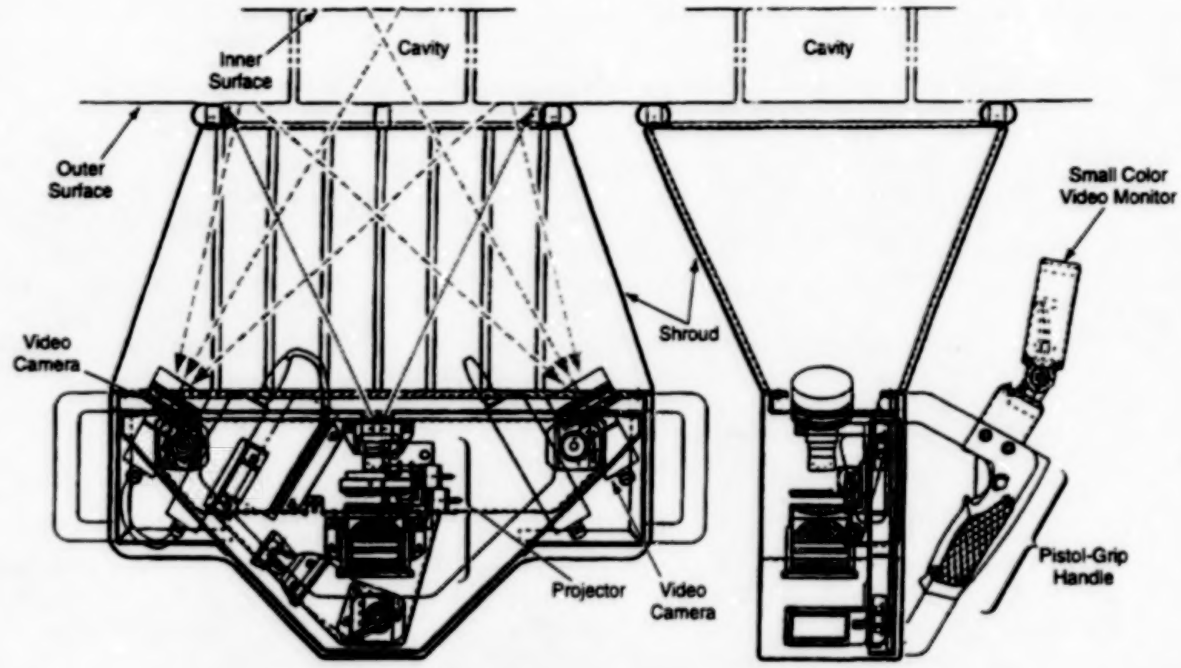

OPTICAL LAYOUT

HAND-HELD TOOL IN USE

Using a Hand-Held Shop Tool that contains a camera and a projector, the technician measures a tile cavity in less than 1 second. Previously, it was necessary to make and use a plaster model in a tedious, messy process that took as long as 30 hours and yielded marginal accuracy.

A hand-held optoelectronic shop tool measures cavities of the order of 6 in. (15 cm) in length and width, 2 to 4 in. (5 to 10 cm) in depth, with nominally flat side walls, and either curved or flat outer and inner surfaces. The system is called the Tile Cavity Measurement System (TCMS) because in the initial application for which it was developed, the cavities are those created by removal of space shuttle insulating tiles. In that application, the data acquired by the system are used in computer-aided design (CAD) and in computer-aided manufacturing (CAM) of new tiles to fit in the cavities. The system can also be used to measure other cavities of similar size and shape.

The hand-held optoelectronic shop tool (see figure) contains a white-light projector that illuminates the surfaces of the cavity with a pattern of stripes. Two high-resolution video cameras mounted on opposite sides of the projector are aimed toward the sidewalls and inner surfaces of the cavity to facilitate viewing the cavity sidewalls from different angles. The reason for using two cameras is simply that one camera would not suffice to view all cavity surfaces. The combined field of view of the cameras is an area of about 10 in. (25

cm) square, which includes the side walls and inner surface of the cavity plus the surrounding outer-surface area. The projector and cameras are connected by a 30-ft (9-m) cable to a mobile workstation, which includes a computer, video display, and the control and interface electronics. The projector and cameras operate under control by the computer, and the outputs of the cameras are digitized and sent to the computer for analysis.

The projector and cameras are mounted on a rigid frame, which includes a shroud that keeps out background light and also serves to stabilize the tool against the cavity outer surface during measurements. The hand-held unit is equipped with handles and a pistol grip for positioning and control. On the pistol-grip handle are menu-selection thumb buttons and a trigger switch to initiate the measurement. A small color video monitor attached to the pistol-grip handle displays menus, video images of the measurement scene, and data.

The projector system includes a solenoid-operated translation stage with a striped pattern mounted on it. In operation, the video cameras acquire a set of four images of the pattern, each translated 1/4 of the stripe width. The entire measurement of a cavity takes less than 1 second. The shifted-stripe-pattern data are then processed by established phase-shifted-fringe-measurement techniques to obtain data from which the cavity surfaces are reconstructed in three dimensions. The data are stored and transferred to other computers in International Graphics Exchange Specification (IGES) format. The data can also be printed.

This work was done by Edward D. Huber and Rick A. Williams of Lockheed Martin Missiles & Space Co. for **Kennedy Space Center**. *Further information is contained in a TSP [see page 1].*

Title to this invention, covered by U.S. Patent No. 5,561,526 has been waived under the provisions of the National Aeronautics and Space Act [42 U.S.C. 2457 (f)]. Inquiries concerning licenses for its commercial development should be addressed to

Edward D. Huber
Lockheed Martin Missiles & Space Co., Inc.
Dept. H1-52, Bldg. 202
Advanced Technology Center
3251 Hanover St.
Palo Alto, CA 94304
(650) 424-3308

Refer to KSC-11727, volume and number of this NASA Tech Briefs *issue, and the page number.*

ASIC for Reed-Solomon Coding and Related Functions

Implemented in the ASIC is a portion of the spacecraft uplink protocol specified in the widely used Consultive Committee for Space Data Systems (CCSDS) international standard.

NASA's Jet Propulsion Laboratory, Pasadena, California

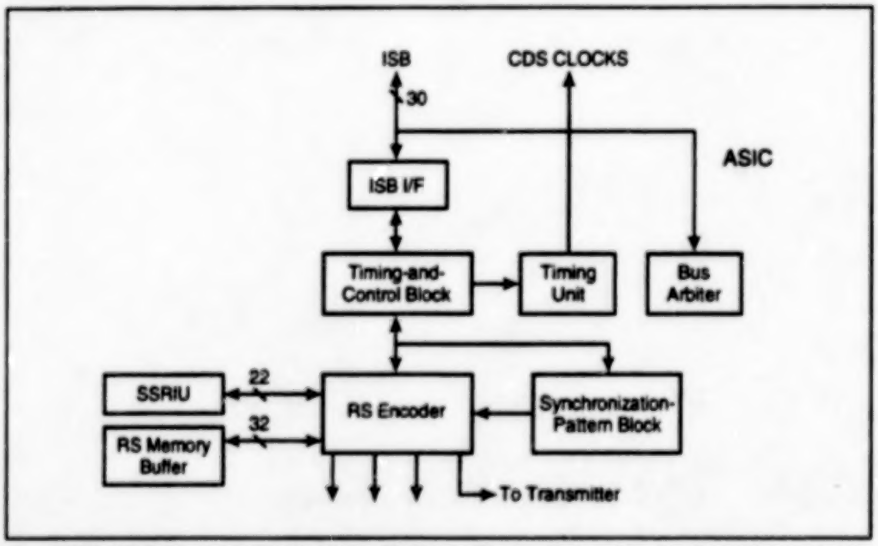

The RSDL ASIC Contains Six Hardware/Software Blocks that perform functions that previously required interfaces to many external circuits.

The Reed-Solomon downlink application-specific integrated circuit (RSDL ASIC) performs Reed-Solomon encoding of telemetry data, internally generates all timing and control signals necessary for the RS encoder, transfers frames of encoded data to a radio transmitter, and performs ancillary timing and control functions. The RSDL ASIC was designed for incorporation into a spacecraft downlink telemetry system, wherein the multiple functions involved in downlinking of telemetry transfer frames previously required interfaces with many discrete circuits and components. The RSDL ASIC may also be adaptable to terrestrial applications (e.g., recording in the entertainment industry) that involve Reed-Solomon encoding.

The RSDL ASIC (see figure) contains six distinct functional hardware/software blocks; an intersubassembly bus interface (ISB I/F), a timing-and-control block, a timing unit (not to be confused with the timing-and-control block), a bus arbiter, a Reed-Solomon (RS) encoder, and a synchronization-pattern block. All of these functional blocks are integrated in a highly efficient manner to fit on one chip. This ASIC operates in conjunction with a solid-state recorder interface unit (SSRIU), a static random-access memory (SRAM) that serves as an RS memory buffer, and a flight computer to forward telemetry transfer frames to the radio transmitter.

The timing-and-control block generates timing and control signals for the rest of the RSDL ASIC (including the timing unit) and keeps track of operational modes. Commands are carried out in the timing-and-control block, which then generates control signals for the synchronization-pattern block and the RS encoder to either shift the synchronization pattern, encode the message, or shift out the RS check bytes. The timing-and-control block also causes the timing unit to set or reset the spacecraft time and to generate the downlink rate used in the RS encoder. It swaps buffers and provides logic to force transfer frames to synchronize with a real-time-interrupt and use a specified downlink buffer thereafter. It captures the time when the first

frame of the downlink buffer is sent out. It provides internal status and interrupt signals for software.

The synchronization-pattern block contains hard-wired logic circuitry that implements a standard synchronization pattern. It shifts data out serially to the RS encoder for every downlink frame, starting with the most significant bit.

The RS encoder block is based on the Berlekamp architecture and implements a standard (255, 233) RS code with an interleave depth of 5. In addition to the RS encoder, the RS encoder block includes a multiplexer to select input from either the synchronization-pattern block or the SSRIU. The RS encoder block is connected directly to the RS memory buffer.

The timing unit generates clock frequencies used throughout a command-and-data subsystem of the spacecraft. The timing unit includes a timing-chain section that converts the main clock signal into clock signals at most of the frequencies needed for that subsystem. From an oscillator with a frequency of 11,944,800 Hz, the timing chain generates a 64.005-Hz signal for the engineering flight computer, a 2,048.148 Hz signal used by a hardware command decoder, a pseudo-16385.185-Hz signal used within the timing unit, and a 32-Hz spacecraft clock signal. The pseudo-16385.185-Hz signal is used in conjunction with counters to generate the 32-Hz signal with high resolution in the following way: A 37-bit counter toggles the upper 32 bits of spacecraft time, giving resolution of 1/32 s. Another counter of 9 bits toggles a 14-bit subsecond time word.

The bus arbiter is the only unrelated block inside the RSDL ASIC. It contains circuitry to arbitrate the ISB between four possible bus masters.

The ISB I/F contains the logic circuitry that serves as an interface between the RSDL ASIC and an external bus arbiter or an engineering flight computer via the ISB. Software that resides in an external computer reads from and writes to internal registers in the ASIC via the ISB I/F. This block indicates whether data are stable and whether data written by the ASIC are captured correctly.

Notable features of the RSDL ASIC (in addition to those mentioned above) include the following:

- It provides a spacecraft clock to keep track of time from 0 to 136 years in 61.03-ms intervals;
- There is a correlation between spacecraft time and the first bit of a defined transfer frame;
- It is easy to reconfigure the RSDL ASIC to other applications: The length of the transfer frame is programmable, software defines the time of the resynchronization of the transfer frames, and the RS encoder can be turned on and off; and
- Software that resides in the flight computer can read and write status and interrupt signals generated by the RSDL ASIC.

This work was done by James A. Donaldson, Huy H. Luong, and Steven H. Wood of Caltech for **NASA's Jet Propulsion Laboratory**. *Further information is contained in a TSP [see page 1].*

In accordance with Public Law 96-517, the contractor has elected to retain title to this invention. Inquiries concerning rights for its commercial use should be addressed to

Larry Gilbert, Director
Technology Transfer
California Institute of Technology
Mail Code 315-6
Pasadena, CA 91125
(818) 395-3288

Refer to NPO-19614, volume and number of this NASA Tech Briefs *issue, and the page number.*

Hardware-Command-Decoding ASIC

Advantages include compactness and low power consumption.

NASA's Jet Propulsion Laboratory, Pasadena, California

A hardware-command-decoding application-specific integrated circuit (HCD ASIC) is designed to decode digital command signals transmitted from a ground station to a spacecraft (uplink commands). Implemented in the ASIC is a portion of the spacecraft uplink protocol specified in the widely used Consultative Committee for Space Data Systems (CCSDS) international standard. A terrestrial version might be useful, for example, in decoding digital command signals for a mobile robot. The HCD ASIC performs functions that previously required several different circuits, while taking up less room and consuming less power. Implemented on a single silicon-based chip in a 256-pin package, this ASIC resists both permanent damage and single-event upsets (bit-flips) produced by ionizing radiation. Tested ASICs are available to users.

This ASIC is designed to operate in conjunction with (1) an engineering flight computer (EFC) connected via an inter-

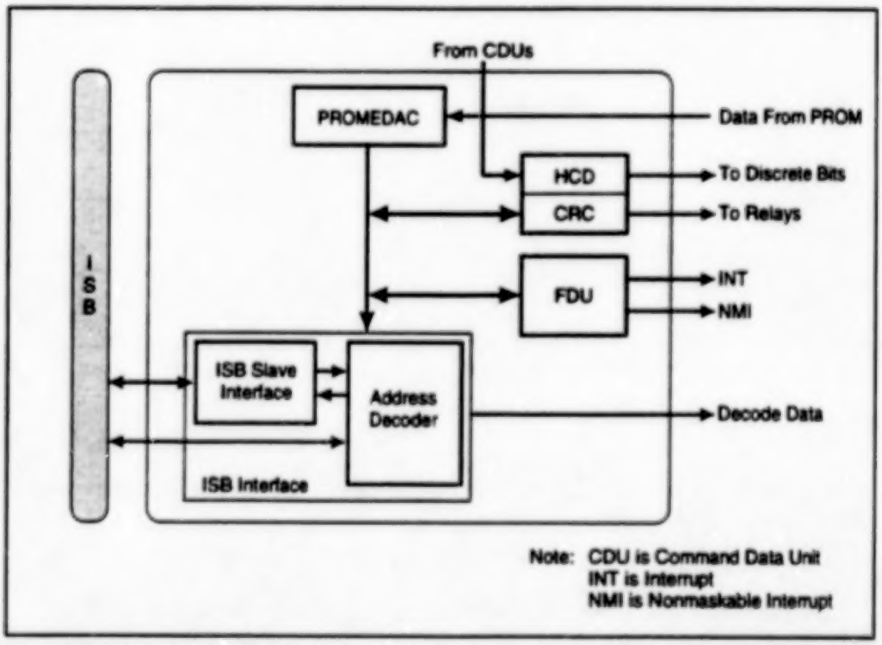

The HCD ASIC performs functions that previously required several different circuits, while taking up less room and consuming less power.

subassembly bus (ISB), (2) critical relay controllers (CRCs), and (3) a start-up programmable read-only memory (PROM). The figure shows the hardware and software functional blocks of the HCD ASIC. In addition to the HCD block, this ASIC contains a block that performs error detection and correction (EDAC) on data that comes from the PROM, a CRC block, an ISB interface block, and a fault-detection unit (FDU). The blocks are integrated in a highly efficient manner to make them fit together on the single chip. A key feature of this ASIC is the ability to accelerate processing in the detection of "start" data sequences and in EDAC, using parallel processing. Another key feature of this chip is the use of the double-buffer method for read/write/status and for resolving overruns of data.

The data from the PROM are in the form of 16-bit words with 6 parity bits. The PROMEDAC corrects any single-bit error and signals to the ISB bus master that it has done so. When the PROMEDAC finds an uncorrectable error, it gives notice to that effect by sending out a "bad" parity signal on the data-bus portion of the ISB.

The FDU includes a watchdog timer and provides interrupt-control support, reset control, and eight discrete outputs that facilitate the exchange of information on the integrity and operational condition of the system.

The ASIC receives a serial, digital data stream as well as a clock signal and a "lock" signal from the uplink data receiver. Two parallel-processing algorithms are used in the HCD block, where traditionally a serial process has been used. "Start" detection is performed by checking the 32 most recent bits of data with the acquisition sequence followed by the "start" sequence. EDAC is also performed by using Perlman's (1980) serial algorithm in a parallel process. A search of uplink data is performed, depending on the "active" or "inactive" state of the HCD. Whenever the "lock" signal is not present, the ASIC goes into the "inactive" state and ignores the uplink. When the "lock" signal appears, the ASIC goes into the "search" state and starts searching uplink data for the "start" sequence. It then goes into the "decode" state and starts decoding code blocks.

EDAC is performed on each code block, and the code block is placed in a data buffer accessible via software. A "tail" sequence forces the ASIC back into the "search" state. Software must fetch a code block from the data buffers (described below) and perform the format checks and interpretation of data. The ASIC presents code blocks to software that pieces them together to form larger frames.

The ASIC contains two data buffers that are used to pass each uplink code block to the software. Each buffer consists of four 16-bit registers and can hold one 64-bit code block. These two data buffers enable the software to read one buffer while the hardware loads the other buffer.

The CRC block communicates directly with the HCD block. It contains data on the state of the command-and-data subsystem of the spacecraft and on the configurations of other parts of the spacecraft. The CRC block includes CRC and EFC mask registers, into which data are written from the ground by use of a specific transfer-frame format. The CRC block includes an EFC/CRC interface that comprises three registers that store 24 volatile CRC bits. These bits are readable and writable through the ISB. An HCD/CRC interface also provides 24 nonvolatile control of relays. Relay state may be changed ahead through the ISB.

The ISB interface connects the ASIC to the outside world through the ISB bus. It also serves as the main interface between the EFC and the command-and-data subsystem. It generates all necessary ISB bus timing signals.

This work was done by Gary S. Bolotin, James A. Donaldson, Huy H. Luong, and Steven H. Wood of Caltech for **NASA's Jet Propulsion Laboratory**. *Further information is contained in a TSP [see page 1].*

In accordance with Public Law 96-517, the contractor has elected to retain title to this invention. Inquiries concerning rights for its commercial use should be addressed to

Larry Gilbert, Director
Technology Transfer
California Institute of Technology
Mail Code 315-6
Pasadena, CA 91125
(818) 395-3288

Refer to NPO-19615, volume and number of this NASA Tech Briefs *issue, and the page number.*

ASIC Physical Layout for the HCD ASIC

HCD ASIC performs a number of functions at unprecedented speed.

NASA's Jet Propulsion Laboratory, Pasadena, California

An integrated circuit (IC) physical layout has been developed for the HCD ASIC — an application-specific integrated circuit that decodes digital command signals transmitted from a ground station to a spacecraft (uplink commands). The HCD ASIC is described in "Hardware-Command-Decoding ASIC" (NPO-19615), which appears elsewhere in this issue of *NASA Tech Briefs*. The present physical layout will be converted to a mask for IC fabrication of the HCD ASIC.

The physical layout has been extensively simulated for its functions of receiving and decoding the uplink commands through a programmable read-only memory (PROM) interface, including conversion of the command data from the serial uplink format to parallel format. At the same time, the HCD ASIC provides detection of some triple bit errors, detection of all double bit errors, and correction of all single-bit errors in the uplink commands, plus detection of hardware faults, all at unprecedented speed. Another unique feature is the use of the double-buffer method for read/write and status for resolving overruns.

This work was done by Gary S. Bolotin, James A. Donaldson, Huy H. Luong, and Steven H. Wood of Caltech for **NASA's Jet Propulsion Laboratory**. *Further information is contained in a TSP [see page 1].*

In accordance with Public Law 96-517, the contractor has elected to retain title to this invention. Inquiries concerning rights for its commercial use should be addressed to

Larry Gilbert, Director
Technology Transfer
California Institute of Technology
Mail Code 315 - 6
Pasadena, CA 91125
(818) 395-3288

Refer to NPO-19628 , volume and number of this NASA Tech Briefs *issue, and the page number.*

Estimating Attitude From GPS Measurements on One Antenna

The antenna boresight direction can be estimated to within approximately ±15°.

NASA's Jet Propulsion Laboratory, Pasadena, California

A technique for estimating the boresight direction of a Global Positioning System (GPS) receiver antenna involves utilization of the relationship between the strengths of received signals and the direction-dependent antenna gain pattern. The technique is fundamentally different from, and much less precise than, other attitude-determination techniques based on interferometry with multiple antennas. The major advantage of this technique is that it quickly gives a coarse estimate, using data from only one antenna. The coarse estimate is not suitable for fine-attitude applications like aiming a telescope or a laser beam, but it can be used, for example, to guide the orientation of a broad-beam communication antenna, to aim a solar panel, or to initialize a fine attitude-determination algorithm or instrument.

The technique is most easily practiced in the case of an antenna with a broad radiation pattern in which the gain decreases monotonically with increasing angle off boresight. The GPS receiver used in this technique must be one that generates data on the signal-to-noise ratio (SNR) of the signal received from each GPS satellite that it tracks. Once the GPS receiver has computed its position from the received GPS signals, the direction to each tracked GPS satellite is known as a byproduct.

The SNR of the signal received from each tracked GPS satellite is taken as a crude measure of the relative strength of the signal and, as such, is used as a weighting value to obtain a vector sum: The unit vector in the known direction to each tracked satellite is multiplied by the SNR for that satellite. The sum of such scalar-vector products for all the tracked satellites is a vector, the direction of which is taken to be the estimated antenna boresight direction. The length of the vector also constitutes ancillary information about the geometric properties of the constellation of tracked GPS satellites.

If only one GPS satellite is being tracked, then the estimated boresight points directly at that satellite; such an estimate is usually erroneous, but it could be helpful in finding other satellites to track and thus obtain a better estimate. When six to eight GPS satellites are being tracked, the estimated boresight differs from the actual boresight by no more than about 15°.

This work was done by Charles Dunn and Courtney Duncan of Caltech for **NASA's Jet Propulsion Laboratory**. *Further information is contained in a TSP [see page 1].*
NPO-20323

Computer System for Managing Construction Projects

An automated system of computer hardware and software has been developed for managing construction projects at Stennis Space Center. This system replaces an older collection of paper-based subsystems, wherein documents were copied, filed, and distributed in labor-intensive processes. Data collected in the older system were not readily accessible, cross-referencing of information in conjunction with changes was difficult, and there was no way of evaluating effects of changes on schedules. The present system includes a commercially available server and workstations running software constructed largely from commercially available office, database, graphical, and spreadsheet software. The system features several data bases with a user-friendly interface, which provides on-line help, plus "intelligent" forms for electronic reporting in standard formats. Drawings and specifications can be retrieved, and "redline" comments can be added. Change packages can be reviewed on-line from remote locations. The system provides security through control of access according to the user's authority to initiate, review, or determine the statuses of change packages and schedules.

This work was done by Catherine L. Farve of Lockheed Martin for **Stennis Space Center**. *Further information is contained in a TSP [see page 1].*
SSC-00061

Books and Reports

Performance of a Soft Digital-Data-Transition Tracking Loop

A report discusses the performance of a soft digital-data-transition tracking loop (DTTL) in a radio receiver that recovers digital data conveyed by binary phase-shift keying. The DTTL is used as a symbol synchronizer; it provides symbol timing to essential parts of the receiver. The DTTL includes a quadrature channel and an in-phase channel, which contains a transition detector with a hyperbolic-tangent response. The DTTL is said to be "hard" or "soft" in the special case of high or low signal-to-noise ratio (high or low SNR, respectively), for which the hyperbolic tangent can be approximated as a hard-limiting or a linear function, respectively. In the report, a mathematical model of a soft DTTL is used to compute two functions that characterize tracking performance: (1) the loop S curve (a normalized expectation value of symbol error as a function of timing error) and (2) the two-sided spectral density of the equivalent additive noise. The performance of the soft DTTL is analyzed by use of these functions and compared with the previously computed performance of a hard DTTL. At low symbol SNRs, the timing jitter of the soft DTTL is found to be less than that of the hard DTTL.

This work was done by Samson Million and Sami Hinedi of Caltech for **NASA's Jet Propulsion Laboratory**. *To obtain a copy of the report, "Tracking Performance of the Soft Digital Data Transition Tracking Loop," see TSP's [page 1].*
NPO-20154

BLANK PAGE

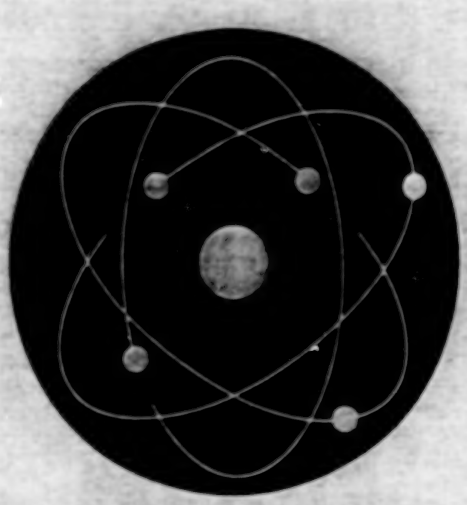

Physical Sciences

Hardware, Techniques, and Processes

Books and Reports

BLANK PAGE

Software Models Processes in a Gaseous Chemical Reactor

A simple, volume-averaged model provides guidance for designing reactors.

Ames Research Center, Moffett Field, California

The Simple Analysis of Materials Processing Reactors (SAMPR) computer code is meant for the analysis of plasma and nonplasma processes used in manufacturing semiconductors. The code can also be used to analyze any chemical-processing reactor with gaseous (but not liquid) streams.

The code implements a mathematical model that consists of balance equations for the total mass, mass of individual chemical species, and gas energy. In the case of plasma reactions, a plasma power balance is also included.

The balance equations are volume-averaged; in other words, they represent a zero-dimensional (0-d) analysis. For this analysis to be valid, the reactor contents must be well mixed and not exhibit significant gradients of species concentrations or gas temperatures in any part of the reactor. Such perfect mixing conditions can be found in reactors used in chemical process industries. Such ideal conditions may not exist in reactors used for etching, deposition, annealing, or performing any other functions in the course of manufacturing integrated circuits. Nevertheless, approximate solutions to somewhat idealized reactor conditions may be valuable in estimating overall conversion efficiency of feedstock, effluent concentrations, and energy utilization.

SAMPR provides volume-averaged electron density, electron temperature, and concentrations of radicals and ions as functions of pressure, input power, and flow rates. Obviously, detailed information on the departure from uniformity of the plasma, and on fluxes of radicals and ions near a wafer in the reactor is lost in such a global model, but quantitative behavior of the plasma as a function of system parameters or the so-called "scaling laws" can be obtained very rapidly. Generation of such valuable knowledge with minimal computational resources is the attraction of this simple approach.

Also, the results obtained from a 0-d model can provide guidance for further multidimensional simulations. Usually, in a semiconductor-processing situation, the numbers of chemical species and reaction pathways are large. Multidimensional analysis with a large set of reactions and species is computationally intensive. A 0-d analysis in such a case can be used effectively in a systematic study to generate a "reduced chemistry set" that provides reasonable results.

This work was done by M. Meyyappan of **Ames Research Center** *and T. R. Govindan of Applied Research Laboratory. Further information is contained in a TSP [see page 1].*

Inquiries concerning rights for the commercial use of this invention should be addressed to the Patent Counsel, Ames Research Center [see page 1]. Refer to ARC-13392.

Carbon/Carbon Shield/Antenna Structure

This strong, lightweight structure could withstand high temperature.

NASA's Jet Propulsion Laboratory, Pasadena, California

A proposed lightweight, off-axis reflector structure for a microwave communication antenna would be made of a carbon/carbon composite material. The structure was conceived for use aboard the Solar Probe spacecraft, where it would also serve as a shield to protect the spacecraft against solar radiation at perihelion. The basic concept of the carbon/carbon reflector structure could be also adapted to design lightweight, strong, off-axis reflector structures for antennas to be used on Earth.

Carbon/carbon was chosen as the class of structural materials because such materials offer a combination of light weight, high strength, good radio-frequency (RF) reflectance properties, and low mass loss at high temperatures. Results of tests of candidate materials suggest that the proposed shield/antenna structure would function well at a temperature greater than 2,000 K. The major drawback of materials in this class is that they are expensive.

In the original Solar Probe application, the dual use of the structure as a solar shield and antenna reflector was made possible by a fortuitous combination of optimum shield and antenna shapes that was effected by designing the spacecraft trajectory to obtain Sun/spacecraft/Earth quadrature at spacecraft perihelion. The combined shield/antenna would also enable a reduction of overall spacecraft diameter. According to an older design concept, the solar shield would be a separate, conical structure and the antenna reflector would lie within the shadow of the shield. The overall spacecraft diameter according to that concept would be 4 meters. The overall diameter according to the proposed simplification would be reduced to 1 meter, and the overall mass and cost of the spacecraft would be concomitantly smaller. Of course, whether or not such simplification and reduction in size could be effected in other applications would depend on the geometries and design and operational requirements specific to those applications.

This work was conceived by James Randolph of Caltech for **NASA's Jet Propulsion Laboratory**. *Further information is contained in a TSP [see page 1].*
NPO-20318

Automated Calibration of Temperature Transducers

An automated system of laboratory equipment and computer hardware and software reduces the time that technicians must spend in calibrating temperature transducers. The laboratory equipment includes a controlled-temperature bath, two digital multimeters for processing the outputs of two temperature transducers at a time, and standard interface bus circuitry for controlling and monitoring the bath and the multimeters. The operation of the laboratory equipment is controlled by equipment-specific software on a computer that runs Windows 95 and is equipped with

a standard general-purpose interface bus circuit card. A technician specifies data points for calibration, and thereafter the software controls the calibration process. The process includes timed advances to subsequent temperatures and holding periods for stabilization at calibration temperatures, with a sampling period of 1 second. The technician can leave the system unattended during the calibration process. Using manual techniques, it usually takes about half a day to calibrate two temperature transducers at three data points; using this system, it takes about two hours.

This work was done by Timothy Joe Pagan of United Space Alliance for **Kennedy Space Center**. *Further information is contained in a TSP [see page 1].*
KSC-11988

Solar/Infrared Aerobots for Exploring Several Planets

A report discusses a class of balloon-borne robotic instrumentation systems that have been proposed for use in exploring Venus, Jupiter, Saturn, Uranus, and Neptune. The balloons would be of the Montgolfier type; that is, buoyancy would be achieved through heating of atmospheric gases contained in the balloons at ambient pressures. However, unlike the familiar fire-heated hot-air balloons invented by the Montgolfier brothers, the proposed balloons would be heated primarily by the Sun during the day and by infrared radiation from relatively warm planetary surfaces at night. The proposed balloons would be modified versions of solar/infrared-heated Montgolfier balloons that were flown in the upper stratosphere of the Earth by the French space agency CNES during the 1980s. The lower parts of those balloons were made of infrared-transparent polymeric materials to admit infrared radiation from below; the upper inside surfaces were blackened to maximize absorption of the admitted infrared radiation, and the upper outside surfaces were aluminized to minimize radiation of heat to outer space. During the day, the balloons would rise high due to solar heating. At night, the balloons would sink lower, with the descent slowed by heating due to compression of the contained gases, as well as by heating from lower planetary radiation.

This work was done by Jack Jones, Matthew Heun, and Kerry Nock of Caltech for **NASA's Jet Propulsion Laboratory**. *To obtain a copy of the report, "Solar Infrared Balloons for Venus, Jupiter, Saturn, Uranus, and Neptune," see TSP's [page 1].*
NPO-20264

Books and Reports

Analysis of Stresses and Deflections in RTDs

A report presents an analysis of stresses and deflections in resistance temperature detectors (RTDs) of various model numbers with standard sizes and shapes. The RTDs are assumed to be installed in pipes that contain flows of oxygen and hydrogen in a test facility at Stennis Space Center. The analysis, performed in a spreadsheet format, involves calculation of maximum stresses and deflections for each RTD under specific fluid conditions. The drag force is entered as a circular reference in the spreadsheet and must be calculated iteratively. The equation for drag force is used to calculate the allowable fluid density for a given velocity. The deflection of the RTD at the inner pipe wall is also compared with the maximum allowable deflection at that point. The output of the analysis is a curve, for each RTD model and size, of fluid density versus flow speed. On the basis of allowable stress and deflection, it is deemed to be safe to operate an RTD at any point below its curve. Thus, the collection of curves serves as a guide for preliminary selection of RTDs for the facility.

This work was done by Michael Jee of Lockheed Martin for **Stennis Space Center**. *To obtain a copy of the report, "RTD Stress Analysis for the E-1 Test Facility," see TSP's [page 1].*
SSC-00064

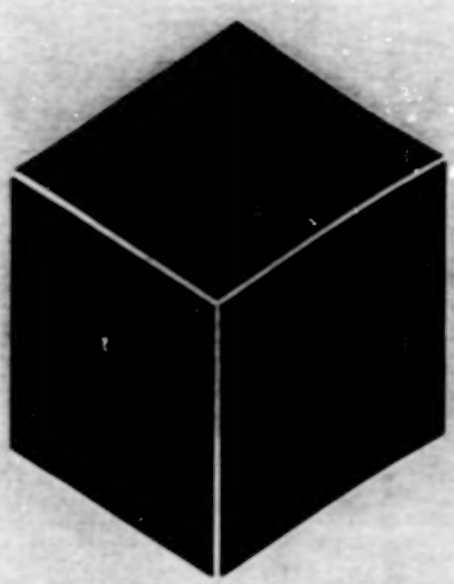

Materials

Hardware, Techniques, and Processes

Books and Reports

BLANK PAGE

Reducing CTE Mismatch Between Coatings and Si-Based Ceramics

Coating compositions would be altered and/or intermediate coats would be used.

Lewis Research Center, Cleveland, Ohio

Two techniques have been proposed to reduce thermal-expansion mismatches between (a) substrates made of silicon, silicon-based ceramics, and silicon-based-ceramic composite materials and (b) surface coats that protect the substrates against chemical attack in oxidizing and/or corrosive environments. Typical substrate materials include SiC/Si composites. A typical coating material is mullite ($Al_6Si_2O_{13}$), which can protect silicon-based substrates against water-free oxidizing and corrosive environments. Mullite can also be applied as intermediate coating layers to relax stresses and enhance the adhesion of overlying protective layers of zirconia (ZrO_2) or nonstoichiometric anorthite (stoichiometric composition $CaAl_2Si_2O_8$). The coefficients of thermal expansion (CTEs) of mullite and of some other typical oxide coating materials are greater than the CTEs of silicon-based substrates and, as a result, the coatings tend to crack through their thicknesses. The cracks become pathways for the entry of the chemical species from which one seeks to protect the substrates.

In one proposed technique, one or more lower-CTE phase(s) would be incorporated into a mullite coating to reduce the CTE of the coating for a better CTE match with the substrate. Suitable lower-CTE compounds include cordierite ($2MgO.2Al_2O_3.5SiO_2$) and fused silica (see Figure 1). Mullite, cordierite, and fused silica would be chemically compatible with the substrate, with each other, and with typical other oxide coating materials. A composite coating of mullite with cordierite and/or fused silica could be applied by plasma spraying or by a wet chemical process.

The CTE of a polycrystalline material like a mullite/cordierite/fused silica composite can be approximated by a rule of mixtures: $\alpha_c = \sum \alpha_i V_i$, where α_c is the CTE of the composite, α_i is the CTE of the ith constituent, and V_i is the volume fraction of the ith constituent. Initially, the proportions of cordierite and/or fused silica could be chosen to obtain a desired value of α_c according to this rule. However, because of the complexity of the phase composition of the mullite/cordierite/fused silica system, a process of trial and error would likely be necessary to establish the optimum composition.

In the second proposed technique, zircon ($ZrSiO_4$) would be applied as an intermediate layer between a substrate and an overlying protective coating. Optionally, if a dense, crack-free zircon coating could be produced, then it could be used, instead of mullite, as a protective coating, provided that there is no water vapor in the environment. In comparison with mullite, zircon has a CTE closer to the CTEs of the typical substrate constituents SiC and Si. If resistance to water is needed, then a protective coating of zirconia (ZrO_2) or of various silicates could be applied over the zircon layer. Zircon would be chemically compatible with both the protective coating and the thin layer of SiO_2 that typically forms on the surface of an Si-based substrate.

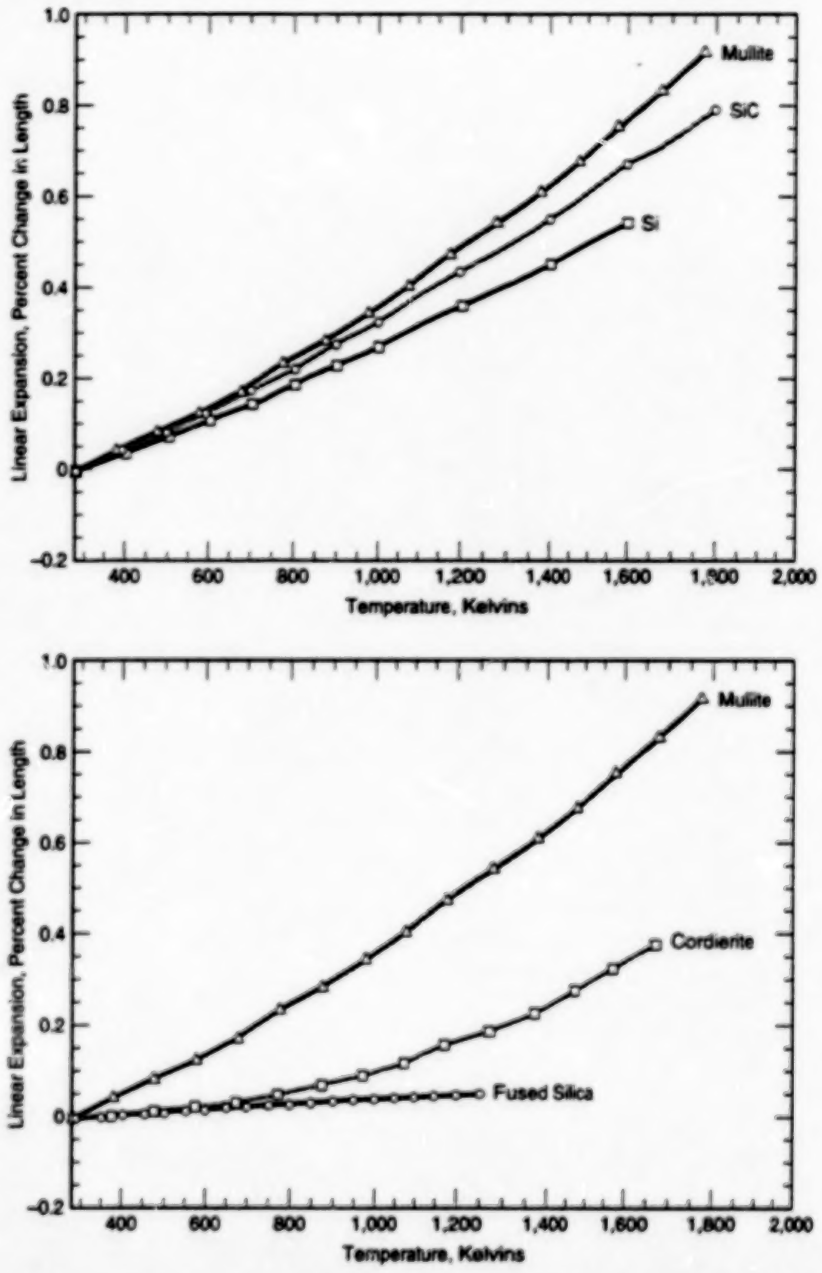

Figure 1. Mismatches Between Thermal Expansions of mullite and of Si and SiC are large enough to cause cracking of mullite coatings on Si-based substrates. Thermal-expansion mismatch can be reduced by incorporating the lower-thermal-expansion material(s) cordierite and/or fused silica into a mullite coating.

Like a mullite/cordierite/fused silica composite coating, a zircon coating could be applied by plasma spraying or by a wet chemical process. Plasma spraying could be complicated by the fact that zircon melts and freezes incongruently, forming cubic zirconia first upon cooling from the liquid phase. It might be necessary to add Y_2O_3 or CaO to the starting composition to stabilize

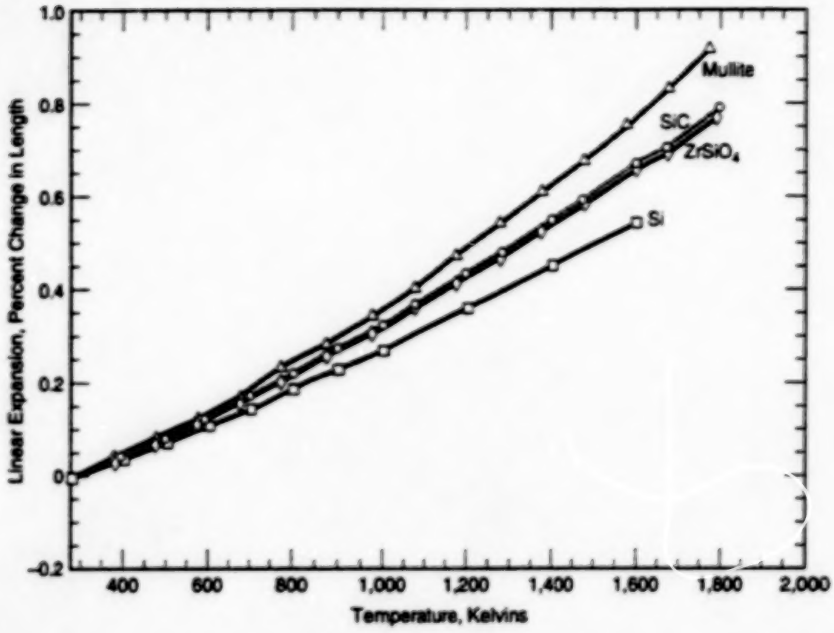

Figure 2. The Thermal Expansion of Zircon matches the thermal expansions of Si and SiC more closely than does the thermal expansion of mullite.

the cubic phase and prevent volumetric changes while allowing the conversion to zircon to take place. Post-spray annealing might be necessary to help the zircon coating reach equilibrium and enhance its stability.

The CTE of zircon is slightly less than that of SiC, though greater than that of Si(see Figure 2). In the case of zircon plasma-sprayed on SiC, the slight difference between the CTEs results in a small compressive stress in the zircon. Inasmuch as the compressive strength of zircon exceeds its tensile strength, this small compressive stress could be advantageous in that it might offset small residual local tensile stresses and thereby help to prevent cracking. As in the first technique, one could incorporate lower-thermal-expansion phases like cordierite and/or fused silica to obtain a lower overall CTE; for example, to obtain a greater compressive stress in a coating on an SiC substrate or to obtain a closer CTE match with an Si substrate.

This work was done by Hongyu Wang of General Electric Co. for **Lewis Research Center**. *For further information, see TSP's [page 1].*

Inquiries concerning rights for the commercial use of this invention should be addressed to NASA Lewis Research Center, Commercial Technology Office, Attn: Tech Brief Patent Status, Mail Stop 7-3, 21000 Brookpark Road, Cleveland, Ohio 44135. Refer to LEW-16393.

Single Crystal Nickel-Base Superalloy

Modified turbine-blade alloy resists fatigue and crack growth.

Marshall Space Flight Center, Alabama

A modified alloy, known as Modified PWA1484, is a single-crystal nickel-base superalloy, developed under a NASA Marshall Space Flight Center contract for use as a turbine blade and vane alloy for the space-shuttle main engine (SSME). This alloy is a modified PWA 1484 composition that uses innovative thermal-process techniques to generate a microstructure specifically tailored for SSME application. The superalloy exhibits significantly better fatigue and crack-growth resistance than previous turbine-blade alloys (such as PWA1480), particularly under severe hydrogen-embrittling conditions.

When compared to the conventional alloy PWA1480, Modified PWA1484 had a high cycle fatigue life that is 100 times greater than PWA1480. Fatigue strength for the new single-crystal nickel-base superalloy was approximately 30 ksi (207 MPa) higher than the previous turbine- blade material.

In other tests, the smooth low cycle fatigue life for PWA1480 was compared to the Modified PWA1484. Fatigue life for the superalloy was more than an order of magnitude greater than PWA1480.

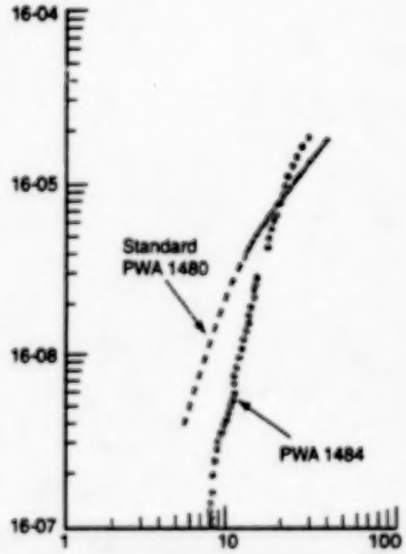

Modified PWA1484 has significantly better fatigue resistance in the critical near-threshold region of the fatigue-crack-growth curve than conventionally used material.

Additionally, this single-crystal nickel-base superalloy was compared against PWA1480 in notched low cycle fatigue. Modified PWA 1484 proved to be 3 to 10 times greater than PWA1480 in notched low cycle fatigue.

When tested for fracture resistance, the Modified PWA 1484 was significantly better in the critical near-threshold region of the fatigue-crack-growth curve than PWA1480. (The results of this test can be seen in the illustration.)

These comparisons show that alloys, such as this single-crystal nickel-base superalloys, will provide better turbine blades and vanes for space-shuttle components, such as high-pressure fuel and oxidizer turbopumps.

This work was done by Daniel P. DeLuca, Charles M. Biondo, and Barrie J. Peters of United Technologies Pratt & Whitney for **Marshall Space Flight Center**. *Further information is contained in a TSP [see page 1].*

MFS-31203

Making Single-Crystal Fibers in a Laser-Heated Floating Zone

Process parameters can be controlled to obtain high-quality single-crystal fibers.

Lewis Research Center, Cleveland, Ohio

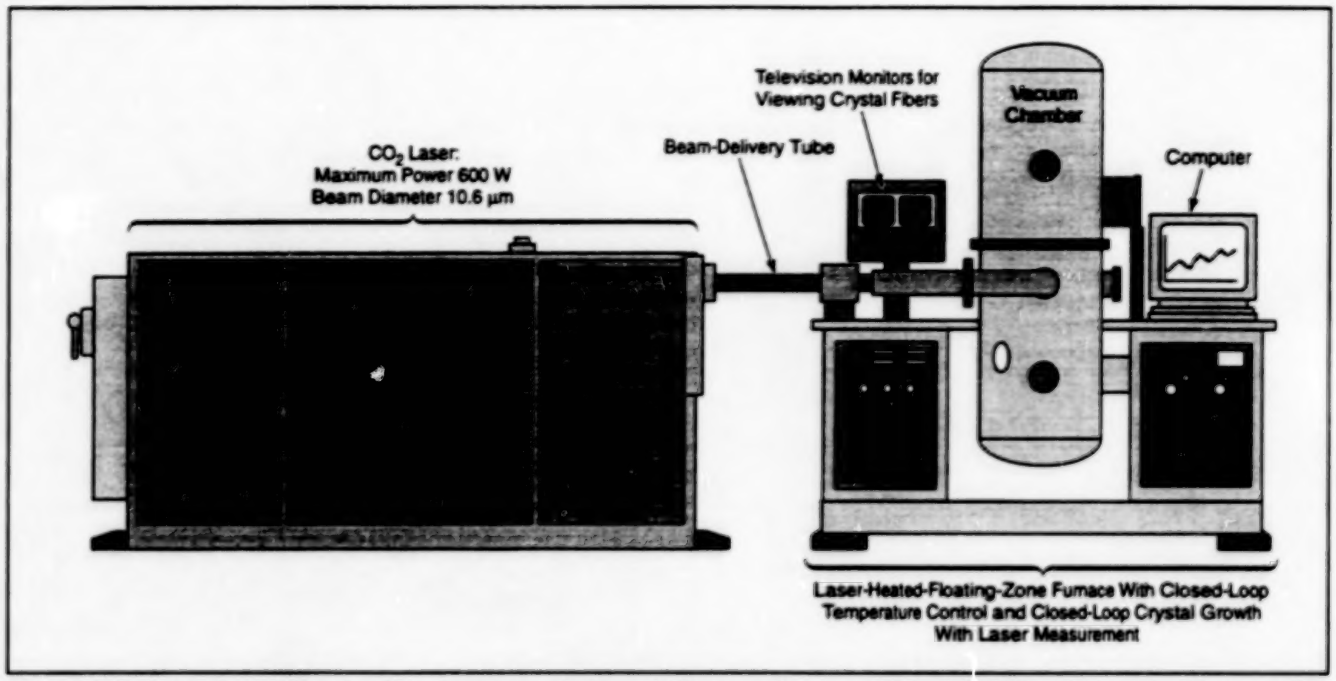

Figure 1. In the **Laser-Heated Floating-Zone Apparatus**, single-crystal fibers can be grown with controlled diameters and specified crystalline orientations.

Figure 1 shows an apparatus for growing a single-crystal fiber by solidification from a floating zone of laser-heated molten material on the tip of a feed rod. The apparatus can be used to produce single-crystal fibers of various highly pure ceramic and metal compositions, controlled crystal orientations, and small, uniform diameters. Such fibers are needed for experimental research on fiber reinforcements for metal-matrix/fiber and intermetallic-matrix/fiber composite materials. Fiber compositions that have been produced thus far include sapphire (Al_2O_3) with and without ternary additions, ZrO_2, and yttrium aluminum garnet (YAG). Typical fiber diameters have ranged from 100 to 250 μm.

Preparation of a feed rod begins with mixing of metallic or ceramic powders with an organic binder. The powders are formulated with a modified stoichiometric composition; that is, the composition is chosen to obtain the desired fiber crystal composition, taking account of anticipated losses of various constituents through differential vaporization from the melt. The mixture of powders and organic binder is extruded to produce the feed rod. The organic binder is typically a commercial water-soluble cellulose ether product formulated to obtain the desired extrusion properties and to vaporize during subsequent laser heating, leaving behind little or no residue.

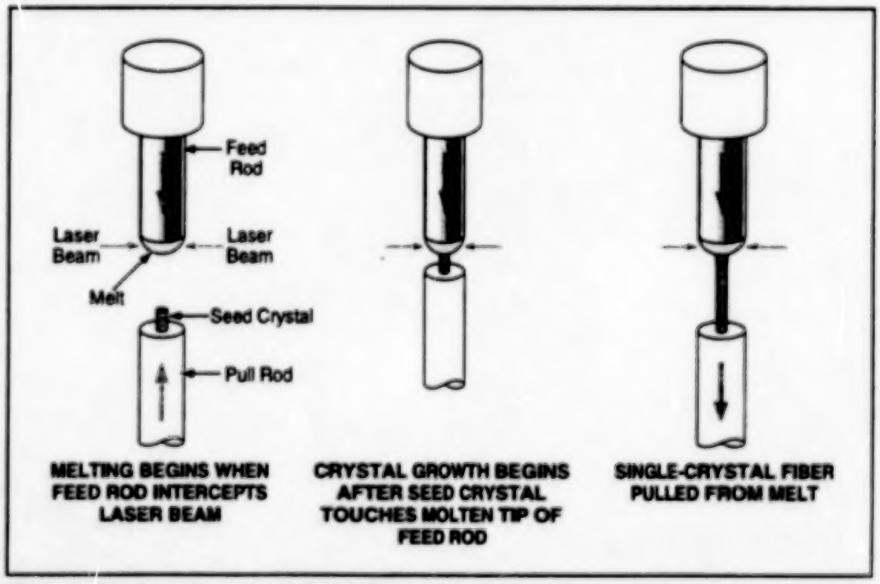

Figure 2. The **Seed Crystal and Feed Rod** are brought together in the laser-heated zone. Once a stable melt has been established, the feed rod is slowly fed into the laser-heated zone while the pull rod is withdrawn to pull out the growing fiber.

The feed rod is mounted vertically on a vertical-translation mechanism inside the vacuum chamber. A seed crystal (which could be a piece of previously grown fiber) is placed in the desired orientation by use of x-ray diffraction for measurement and a goniometer for adjustment. The oriented seed crystal is mounted in the desired orientation on the tip of a pull rod that is collinear with the feed rod and is connected to another, independently controllable vertical-translation mechanism inside the vacuum chamber.

The laser beam is split into two beams aimed at the floating-zone melt location from opposite sides. The tip of the feed rod and the seed crystal on the tip of the pull

rod are slowly brought toward each other and into the laser-heated floating zone, causing them to begin to melt (see Figure 2). Eventually, the molten tips touch and wet each other. Once a stable molten zone with a relatively uniform temperature profile has been established, growth of a single-crystal fiber can begin.

To effect this growth, the feed rod is translated toward the laser-heated zone at one speed while the pull rod is translated away from the laser-heated zone at a different speed. The ratio between the speeds is chosen to obtain the desired change from the diameter of the feed rod to the diameter of the fiber. Ordinarily, one seeks to produce a fiber narrower than the feed rod, so that the pull rod must be translated more rapidly. The translation can be either downward as in Figure 2, or else upward.

A technique called "melt modulation" is used to maintain stability and symmetry in the molten zone. Melt modulation is effected by optomechanically scanning the opposing laser beams back and forth across the feed-rod/fiber axis to obtain more nearly even heating. Melt modulation gives rise to small vibrations that help to stabilize the molten zone. The vibrations also increase thermal agitation and mixing, thereby helping to make the temperature more nearly uniform throughout the melt. The vibrations also help to shake bubbles out of the melt; without the vibrations, small bubbles tend to coalesce into one large bubble in the molten zone, with consequent disruption of crystal growth. The frequency of vibration can be adjusted to avoid mechanical resonances and minimize vibration of the growing crystal. Typically, the optimum frequency lies between 30 and 50 Hz.

This work was done by Frank Ritzert and Leonard Westfall of **Lewis Research Center**. *For further information, see TSP's [page 1].*

Inquiries concerning rights for the commercial use of this invention should be addressed to NASA Lewis Research Center, Commercial Technology Office, Attn: Tech Brief Patent Status, Mail Stop 7–3, 21000 Brookpark Road, Cleveland, Ohio 44135. Refer to LEW-16539.

Books and Reports

Muscle Wires for Planetary-Exploration Robots

A report proposes the use of muscle wires as mechanical actuators for planetary-exploration robots. Muscle wires are commercially available in kit form in the hobby market, and have been described (though not explicitly called "muscle wires") in previous articles in *NASA Tech Briefs*. A muscle wire is made of a shape-memory alloy. By sending a sufficient electric current along the wire, one can heat the wire above its transition temperature, causing it to change length. When the current is turned off, the wire cools, returning to its original length. The aspects of muscle wires that make them attractive for planetary-exploration robots are low mass, simplicity, and the ability to exert large tensile forces (thousands of times their own weights); in these aspects, muscle wires are superior to conventional electric motors. Moreover, because of their low thermal masses, muscle wires would respond to turn-on and turn-off of currents rapidly enough for the actuation frequencies needed in planetary-exploration robots.

This work was done by Kumar Ramohalli of Caltech for **NASA's Jet Propulsion Laboratory**. *To obtain a copy of the report, "Muscle Wires for Efficient Planetary Exploration Robots," see TSP's [page 1].*
NPO-20194

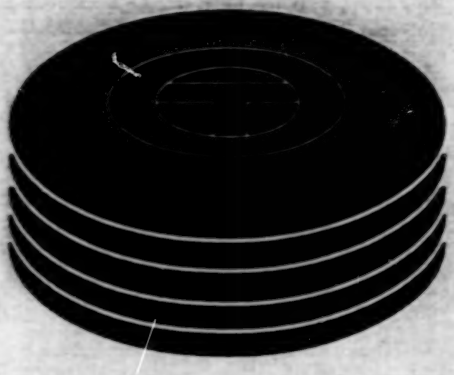

Computer Programs

Electronic Systems

BLANK PAGE

Computer Programs

These programs may be obtained from COSMIC. Please contact

COSMIC®
Computer Services Annex
University of Georgia
Athens, GA 30602
Telephone No. (404) 542-3265.

Electronic Systems

Application Specific Integrated Circuit Physical Layout for the RSDL ASIC

An integrated circuit physical layout has been developed for the RSDL ASIC — an integrated circuit that encodes telemetry data and transfers the data (which are grouped together in transfer frames) to a radio transmitter. The RSDL ASIC is described in "ASIC for Reed-Solomon Coding and Related Functions" (NPO-19614), which appears elsewhere in this issue of *NASA Tech Briefs*. The present physical layout will be converted to mask for IC fabrication of the RSDL ASIC. The physical layout has been extensively simulated for its timing, control, bus-arbitration, encoding, and data-transfer functions, which have been summarized in the noted prior article.

This work was done by James A. Donaldson, Steven H. Wood, and Huy H. Luong of Caltech for **NASA's Jet Propulsion Laboratory**. *For further information, see TSP's [page 1].*

In accordance with Public Law 96-517, the contractor has elected to retain title to this invention. Inquiries concerning rights for its commercial use should be addressed to

Larry Gilbert, Director
Technology Transfer
California Institute of Technology
Mail Code 315 - 6
Pasadena, CA 91125
(818) 395-3288

Refer to NPO-19626, volume and number of this NASA Tech Briefs *issue, and the page number.*

BLANK PAGE

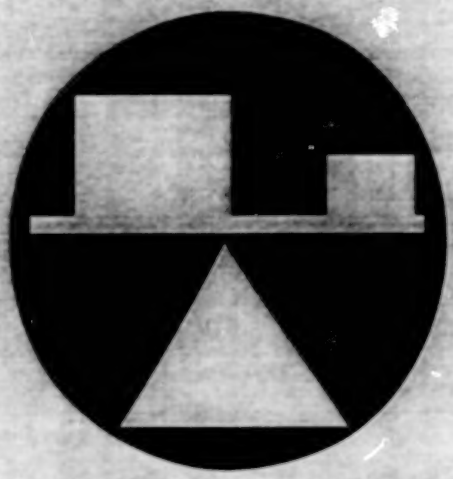

Mechanics

Hardware, Techniques, and Processes

BLANK PAGE

The Modified Fully Utilized Design Method

Solutions are comparable to those obtained by nonlinear optimization techniques.

Lewis Research Center, Cleveland, Ohio

The modified fully utilized design (MFUD) method is undergoing development for use by engineers who favor traditional methods of designing structures over methods based on advanced calculus and nonlinear mathematical programming techniques. Thus far, the MFUD has been developed for trusses, with cross-sectional areas of truss members as design variables. Like nonlinear optimization methods, the MFUD method is iterative, but in comparison with those methods, the MFUD method involves less and simpler computation.

The MFUD method is derived from the fully stressed design (FSD) and fully utilized design (FUD) methods. The FSD method, based on a simple stress-ratio approach, is popular in civil, mechanical, and aerospace engineering. The FSD method is an elegant conceptual tool for arriving at stress-limited designs, but does not provide for displacement constraints, which are imposed with increasing frequency in designing modern structures.

An extension of the FSD method through provision for displacement constraints in addition to stress constraints yields the FUD method. The term "fully utilized design" signifies a design in which the number of active constraints equals or exceeds the number of design variables. One obtains the FUD of a structure by the following procedure:

1. Using the stress constraints only, generate the FSD.
2. Uniformly prorate the FSD to obtain the FUD, using a constant proration factor that satisfies the single most infeasible displacement constraint. For a truss structure, this entails multiplying the cross-sectional areas of all truss members by the same factor to strengthen all the members enough to limit the displacement, as required.

The FUD thus obtained is feasible but can be an overdesign; the weight of the FUD structure can be greater than that of an optimally designed structure.

The MFUD method accommodates both stress and displacement constraints simultaneously. The steps of this method applied to a simple truss structure are the following:

1. Identify the design variables to initiate iterations. Optionally, one can begin iterations from the FSD. For subsequent iterations, the stress constraints are expressed in terms of cross-sectional areas, given by

$$A_i = (F)_{max}/\sigma_{i0}$$

where A_i is the area in question for the ith member, $(F)_{max}$ is the maximum force in ith member under all loading conditions, and σ_{i0} is the maximum allowable stress in the ith member.
2. Identify the displacement constraints violated by the design obtained in step 1.
3. For each displacement constraint identified in step 2, update the design independently to satisfy the constraint. The update process comprises two subprocesses: (1) identification of a subset of design variables pertinent to that constraint and (2) computation, for each member, of a member-weighted parameter, which is a multiplicative parameter based partly on the sensitivity of the constraint-violating displacement to the cross-sectional area of the member. The member-weighted parameter supplants the constant proration parameter of the FUD method. The equations used in these subprocesses are derived from the integrated force method, which was described in "Constructing Finite Elements for the Integrated Force Method" (LEW-16421), NASA Tech Briefs, Vol. 21, No. 7 (July 1997), page 70.
4. Obtain the design update for the structure as the union of all of the designs updated for the constraints in step 3. If any member is affected by more than one of the constraint-updated designs in the union process, the cross-sectional area selected for that member should be the maximum one.
5. Repeat steps 1 through 4 until the design converges. The converged design will satisfy both stress and displacement constraints.

Despite its relative simplicity, and even

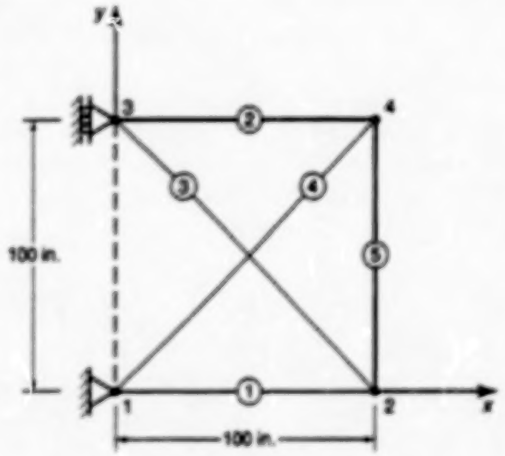

FIVE-BAR TRUSS

Results	MFUD	FUD	SUMT	OC
Optimum Weight, lb	44.817	62.228	45.029	45.016
Member Area, in^2:				
A_1	0.001	1.068	0.001	0.001
A_2	1.475	1.068	1.501	1.499
A_3	0.001	1.068	0.001	0.001
A_4	2.124	1.068	2.119	2.120
A_5	0.001	1.068	0.001	0.001

DESIGN RESULTS

A Five-Bar Truss subject to one load and one displacement constraint was designed by the MFUD and FUD methods and by two optimization methods called "SUMT" and "OC." In this case, the FUD design was about 39 percent too heavy, while the MFUD design was even lighter in weight (more nearly optimum) than were the SUMT and OC designs.

though it does not incorporate an explicit minimum-weight condition, the MFUD method can yield solutions comparable to those obtained by nonlinear optimization techniques (for example, see figure). Even if one still prefers a full optimization, the MFUD method could be used to generate initial designs for subsequent optimization iterations, thereby alleviating some of the computational burden of optimization.

This work was done by Laszlo Berke and Dale Hopkins of **Lewis Research Center**, *Surya Patnaik of Ohio Aerospace Institute, and Atef Genoy of the National Research Council. Further information is contained in a TSP [see page 1].*

Inquiries concerning rights for the commercial use of this invention should be addressed to NASA Lewis Research Center, Commercial Technology Office, Attn: Tech Brief Patent Status, Mail Stop 7–3, 21000 Brookpark Road, Cleveland, Ohio 44135. Refer to LEW-16624.

Magnetostrictive Inertial-Reaction Linear Motors

Fine positioning could be achieved at temperatures from near absolute zero to ambient.

NASA's Jet Propulsion Laboratory, Pasadena, California

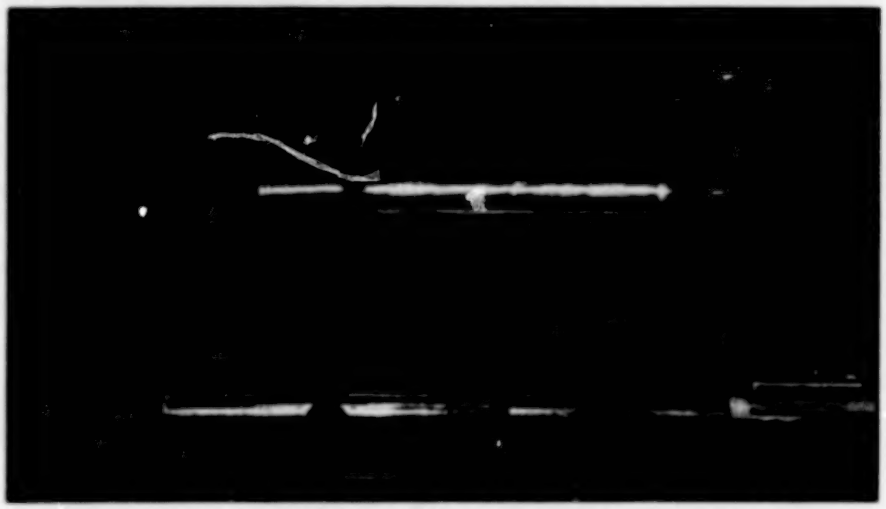

This **Magnetostrictive Inertial-Reaction Motor** is a proof-of-concept model that has been shown to produce incremental motions as small as 100 nm.

Linear-translation motors containing inertial-reaction masses driven by magnetostrictive actuator elements are undergoing development. These motors could be used to make fine position adjustments in diverse scientific and industrial instruments that operate at temperatures ranging from near absolute zero to room temperature; for example, they could be used to drive translation stages in scanning tunneling microscopes that operate at liquid-helium temperature (4 K), or to move cryogenic-temperature optical elements that must be located at long but precise distances from each other (as in interferometers). [These motors should not be confused with proposed magnetostrictive motors that would move in "inchworm" fashion and would be used for similar purposes, described in "Magnetostrictive Actuators for Cryogenic Applications," *NASA Tech Briefs*, Vol. 20, No. 3 (March 1996), page 84.]

An inertial-reaction motor includes a platform that slides along a pair of tracks. One end of an electrically driven linear actuator is mounted on the platform, and a substantial mass (the inertial-reaction mass) is attached to the other end. The actuator can be made to move the mass, rapidly or slowly, along a short range parallel to the track. If the mass is driven with sufficient acceleration that the reaction force overcomes the friction between the platform and the track, then the platform moves a short distance along the track. If, following a rapid stroke in the forward direction, the mass is driven relatively slowly in the reverse direction, then the reaction force is insufficient to overcome friction, and thus the platform remains in the position to which it moved during the forward stroke. By driving the actuator with a sawtooth waveform at the appropriate amplitude and frequency, one can cause the actuator to repeat this action and thus move the platform in a succession of small steps. The total distance traveled can range from a single step to the length of the tracks, which could be as much as 1 m or more in some instruments. The motion can be reversed by inverting the waveform driving the actuator.

The principle of operation as described thus far does not call for any particular type of linear actuator. Heretofore, inertial-reaction motors have been constructed with piezoelectric actuators. However, piezoelectric actuators exhibit diminished performance as temperature decreases into the cryogenic range; at liquid-helium temperatures (about 4 K), piezoelectric actuators perform poorly.

Unlike piezoelectric actuators, magnetostrictive actuators perform well at temperatures from ambient down to 4 K and below; indeed, magnetostrictive actuators reach their performance peaks at cryogenic temperatures, while at room temperature, they produce strokes about 7 times as large as those of comparable piezoelectric actuators. Moreover, if the magnetostrictive linear actuators for cryogenic inertial-reaction motors are constructed with superconducting solenoids, then the conversion of electrical to mechanical energy could be more efficient.

The feasibility of magnetostrictive inertial-reaction motors has been demonstrated in tests of such a motor built with a commercial room-temperature magnetostrictive actuator (see figure). Incremental motions as small as 100 nm have been achieved. With further development, it should be possible to achieve increments as small as 10 nm.

This work was done by Christian Lindensmith and Robert Chave of Caltech for **NASA's Jet Propulsion Laboratory**. *Further information is contained in a TSP [see page 1].*
NPO-20153

Automated PreLaunch Loads Estimation (APLLE)

A computer program quickly and accurately calculates prelaunch ground-wind loads for different launch-vehicle configurations.

Marshall Space Flight Center, Alabama

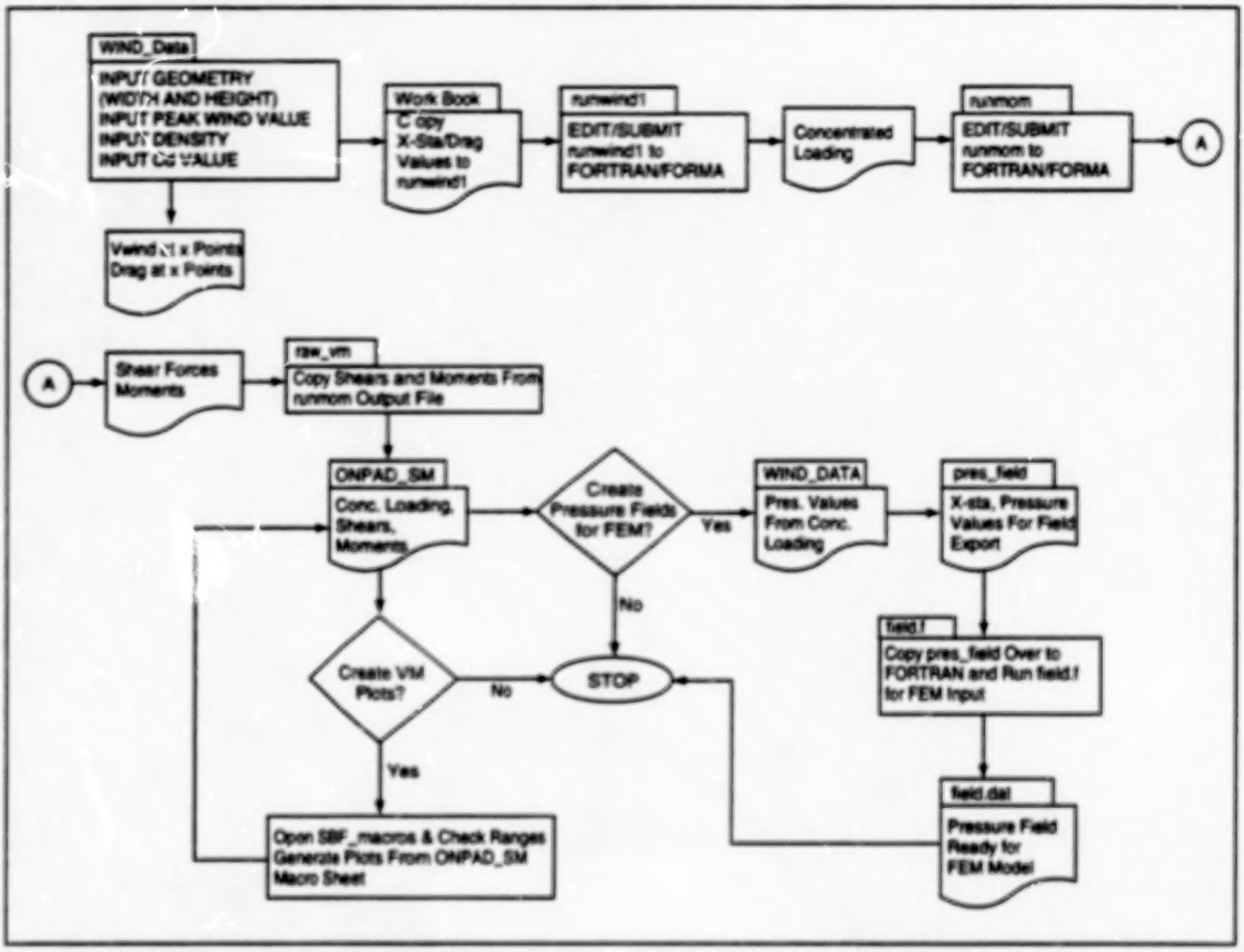

The **Automated PreLaunch Loads Estimation (APLLE)** procedure provides quick and accurate load estimations for a variety of structures.

Over the past year, the Structural Dynamics and Loads Branch of Marshall Space Flight Center has been calculating prelaunch ground winds for several different launch-vehicle configurations. Engineers developed a computer programming system to streamline the analysis cycle.

This documented procedure, known as Automated PreLaunch Loads Estimation (APLLE), uses a spreadsheet, word processor, and FORTRAN computer programs to provide quick and accurate load estimations. APLLE can easily be adapted for structures other than launch vehicles.

APLLE combines the input of structure geometry (width and height), a reference peak-wind value, a reference altitude and density, and an estimated drag-coefficient value based upon the shape of the structure. With these inputs, APLLE calculates a concentrated load, cumulative shear, and bending-moment values for a set of discrete points. The spreadsheet macro provides rapid diagrams of shear and moment. Additionally, pressures are extrapolated from the concentrated loads to form a pressure field that can be applied to a finite-element code.

For a free-standing structure, wind loading is the only forcing function other than gravity acting on the vehicle. Calculation of these wind loads assumes the wind load acts as a steady-state load.

Wind loading is divided into two parts: the drag load and the vortex-shedding load. The drag load is assumed to act parallel to the wind vector, and the vortex shedding acts normal to the wind vector. An uncertainty factor of 1.5 is applied to the wind loads to account for vortex shedding and gusts.

This work was done by Samuel B. Fowler and Joseph Brunty of the **Marshall Space Flight Center**. *Further information is contained in a TSP [see page 1].*

MFS-31149

BLANK PAGE

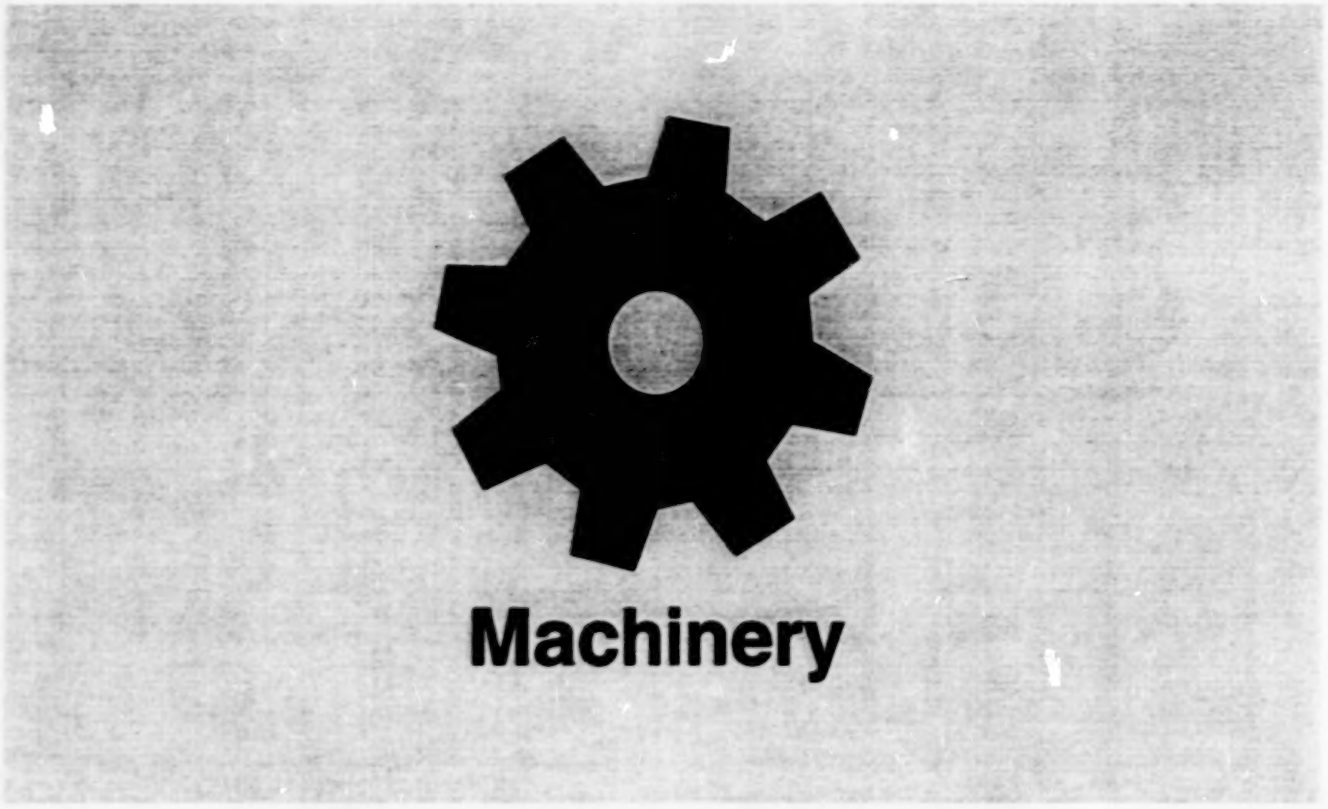

Machinery

Hardware, Techniques, and Processes

Books and Reports

BLANK PAGE

Sensory-Feedback Exoskeletal Arm Controller

Forces and torques are reflected from a robotic manipulator back to the human wearer.

Lyndon B. Johnson Space Center, Houston, Texas

An electromechanical exoskeletal arm apparatus has been designed for use in controlling a remote robotic manipulator arm. The apparatus, called a "force-feedback exoskeleton arm master" (F-EAM) is comfortable to wear and easy to don and doff. It provides control signals from the wearer's arm to a robot arm or a computer simulator (e.g., a virtual-reality system); it also provides force and torque feedback from sensors on the robot arm or from the computer simulator to the wearer's arm. The F-EAM enables the wearer to make the robot arm gently touch objects and finely manipulate them without exerting excessive forces.

The F-EAM features a lightweight design in which the motors and gear heads that generate force and torque feedback are made smaller than they ordinarily would be: this is achieved by driving the motors to power levels greater than would ordinarily be used in order to obtain higher torques, and by providing active liquid cooling of the motors to prevent overheating at the high drive levels.

The F-EAM (see figure) includes an assembly that resembles a backpack and is worn like a backpack, plus an exoskeletal arm mechanism. The F-EAM has five degrees of freedom (DOFs) that correspond to those of the human arm:

1. The first DOF is that of the side-to-side rotation of the upper arm about the shoulder (rotation about axis 1). The reflected torque for this DOF is provided by motor 1 via drum 1 and a planar four-bar linkage.
2. The second DOF is that of the up-and-down rotation of the arm about the shoulder. The reflected torque for this DOF is provided by motor 2 via drum 2.
3. The third DOF is that of twisting of the upper arm about its longitudinal axis. This DOF is implemented in a cable remote-center mechanism (CRCM). The reflected torque for this DOF is provided by motor 3, which drives the upper-arm cuff and the mechanism below it. A bladder inflatable by gas or liquid is placed between the cuff and the wearer's upper arm to compensate for misalignment between the exoskeletal mechanism and the shoulder.
4. The fourth DOF is that of flexion and extension of the elbow. The reflected torque for this DOF is provided by motor 4 and drum 4, which are mounted on a bracket that can slide longitudinally by a pin-and-slot engagement with the upper-arm cuff to compensate for slight variations in the position of the kinematic center of the elbow. Attached to drum 4 is an adapter plate to which is attached a CRCM for the lower arm.
5. The lower-arm CRCM implements the fifth DOF, which is the twist of the forearm about its longitudinal axis. Motor 5 provides the reflected torque for this DOF by driving the lower-arm cuff. A rod transmits twist and torsion between the lower-arm cuff and the hand cuff.

With this system, the motion of the wearer's joints and the reflected torques applied to these joints can be measured and controlled in a relatively simple manner. This is because the anthropomorphic design of the mechanism imitates the kinematics of the human arm, eliminating the need for kinematic conversion of joint-torque and joint-angle data.

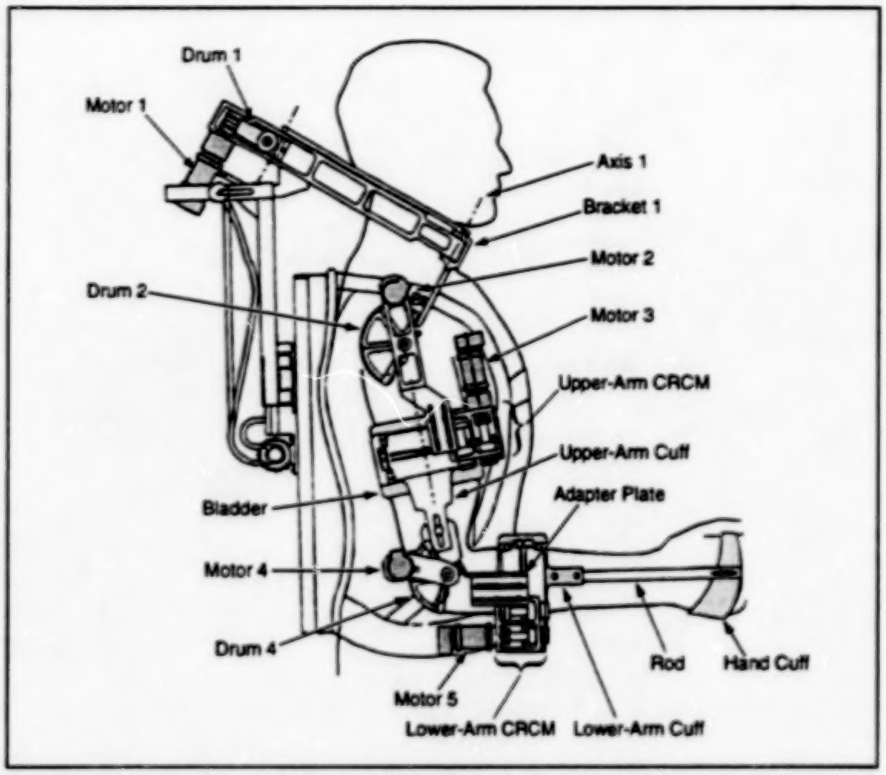

The Force-Feedback Exoskeleton Arm Master is designed for maximum comfort and low weight to minimize wearer fatigue. Its mechanism imitates the kinematics of the human arm.

This work was done by Bin An, Thomas H. Massie, and Vladimir Vayner of Exos, Inc., for **Johnson Space Center**. *Further information is contained in a TSP [see page 1].*

In accordance with Public Law 96-517, the contractor has elected to retain title to this invention. Inquiries concerning rights for its commercial use should be addressed to

Mr. Bin An
Exos, Inc.
2A Gill St.
Woburn, MA 01801
(617) 933-0022

Refer to MSC-22563, volume and number of this NASA Tech Briefs *issue, and the page number.*

Evaluation of a "Smart" Aircraft Control Actuator

Benefits for future aircraft could include decreases in weights, costs, and electromagnetic susceptibility.

Dryden Flight Research Center, Edwards, California

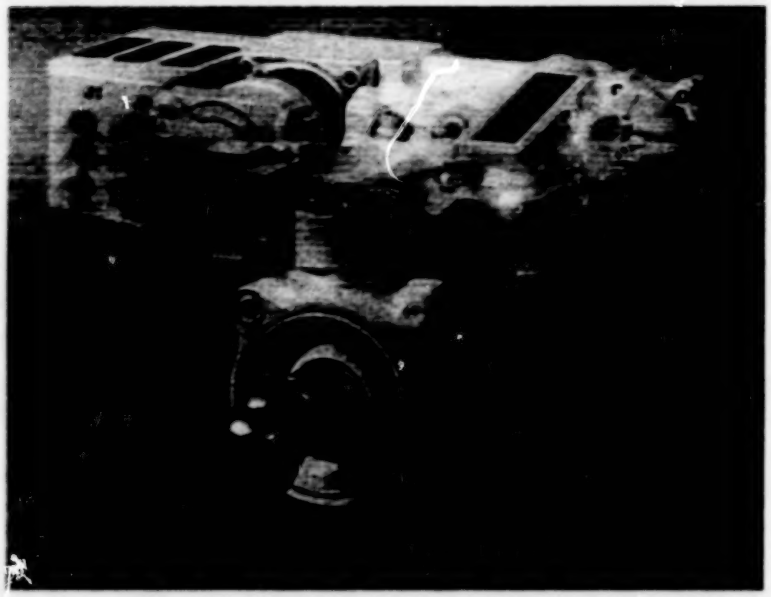

Figure 1. The Smart Actuator includes self-contained control electronics that perform functions that, in older systems, were performed within flight-control computers remote from actuators.

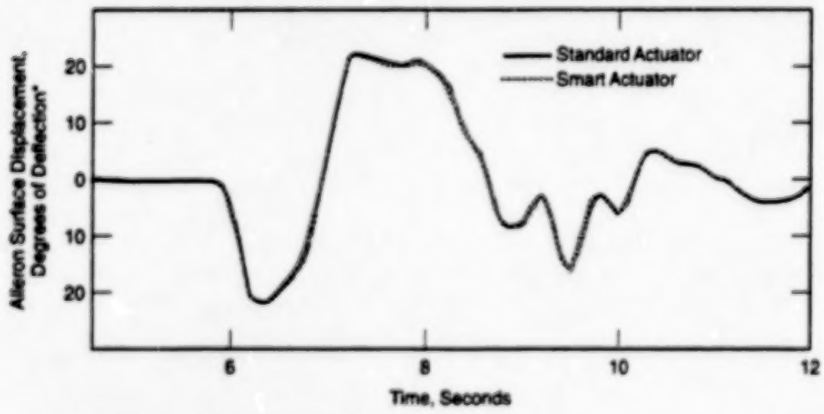

Figure 2. Nearly Identical Performances were exhibited by the smart actuator and the standard F-18 aileron actuator in a flight test. [Aileron reversal ±60° bank angle, 24 kft (7.2 km), 0.4 M, 88 q.]

An aircraft control actuator that incorporates self-contained control electronics has been installed in the F-18 Systems Research Aircraft and evaluated in flight tests. This "smart" actuator is a prototype of fly-by-wire servoactuators for future advanced aircraft.

Fly-by-wire servoactuators now used in military and commercial aircraft are not "smart" in that they do not use self-contained control electronics. Generally, electronic control and monitoring of servoactuators on aircraft are accomplished within separate flight-control computers. As a result, a large amount of wire is needed to operate all the actuators on an aircraft. Especially in a large commercial aircraft, the weight of the wire is significant. Other disadvantages of such a fly-by-wire system include high cost of maintenance, vulnerability to interference by electromagnetic signals (including electromagnetic pulses), and the need for a unique flight-control interface for each actuator.

The smart actuator (see Figure 1) was designed to fit in the left aileron bay of the F-18 airplane. The smart actuator contains two independent electronic channels that perform actuator-control, fault-monitoring, and redundancy-management functions. Communication with the actuator has been simplified by use of standard serial data buses. Instead of wires, optical fibers are used as the communication media.

Installation of the smart actuator on the F-18 airplane necessitated two interface units. These units not only provide the electrical-to-optical interface between the smart actuator and the F-18 flight-control computers, but also provide data to the instrumentation system of the airplane. The use of the interface units also makes it unnecessary to modify the flight-control computers.

The performance of the smart actuator throughout the flight-test program has been exceptional (see Figure 2). Likewise, the fiber-optic data buses used with the smart actuator performed well throughout flight testing. Moreover, the smart actuator performance was virtually identical to the F-18 production actuator. Although environmental tests revealed that the fiber-optic data buses were thermally sensitive, a maintenance-and-calibration procedure was developed to account for the sensitivities. Fiber optics were found to be satisfactorily reliable, and maintenance was easily performed. No anomalies occurred during the flight tests.

The development and flight testing of the smart actuator have proved that local control and monitoring of servoactuators is possible. Although sensitivities of the fiber-optic data buses were discovered, these sensitivities can be factored into future system designs. The use of fiber optics and serial data buses simplified integration of systems and provided valuable information regarding reliability and maintainability of fiber optics on aircraft. In addition, the use of fiber optics may translate to decreased weights, decreased costs, and decreased electromagnetic susceptibility for future aircraft.

This work was done by Karl Alvarado, Denis Bessette, Dorothea Cohen, Bill Fredriksen, Gordon Fullerton, Don Hermann, Linda Kelly, Doug Lindquist, Dick Klein, Bill McGrory, Harry Miller,

Cynthia Norman, Lyle Ramey, Mauricio Rivas, Karla Shy, Joel Sitz, Daryl Townsend, and Eddie Zavala of **Dryden Flight Research Center**; *Karen Richards of HSI; Gavin Jenney and Bruce Raymond of Dynamic Controls, Inc.; Dave Dawson and Major Dennis Trosen of the U. S. Air Force Wright Laboratories; Sean Donley of the U. S. Navy; and Bob Heegey and Bob Deller of HR Textron. Further information is contained in a TSP [see page 1].*
DRC-96-73

Earthwormlike Exploratory Robots

Mobility would be achieved through coordinated actions resembling peristalsis.

NASA's Jet Propulsion Laboratory, Pasadena, California

Mobile robots that would resemble earthworms have been proposed for use in exploring remote, hostile, or inaccessible terrain surface and subsurface environments. This class of robots would be a special case of the more general class of proposed small, lightweight, relatively inexpensive exploratory robots. To recapitulate: Biomorphic explorers would exploit the emerging technology of biomorphic controls and advanced actuators. They would achieve motion by use of simple electronically or photonically controlled, flexible advanced actuators instead of conventional motors with complex drive trains. The robots would carry advanced microsensors for measuring or detecting specific objects or substances. Animallike combinations of mobility, adaptability, fault tolerance and a limited capability for "learning" would be achieved by integrating the actuators with very-large-scale integrated (VLSI) circuits that would implement neural-network and/or genetic algorithms.

The proposed earthwormlike robots would be flexible in the sense that they would be foldable in segments. The first several segments at one or both end(s) of each robot would generate motion. These segments would be covered with hinged plates connected to interior actuators (see figure). Upon command, the interior actuator in each segment would shorten or lengthen the segment, causing the plates to buckle outward or to move inward to straighten, respectively. A wave of shortening/buckling versus lengthening/straightening, resembling the peristaltic motion of an earthworm, could be generated by sending coordinated, sequential contraction and expansion commands to the actuators in the segments. By this action, the robot could move along the surface or burrow beneath the surface of terrain. The direction of travel could be reversed by reversing the sequence of buckling and straightening.

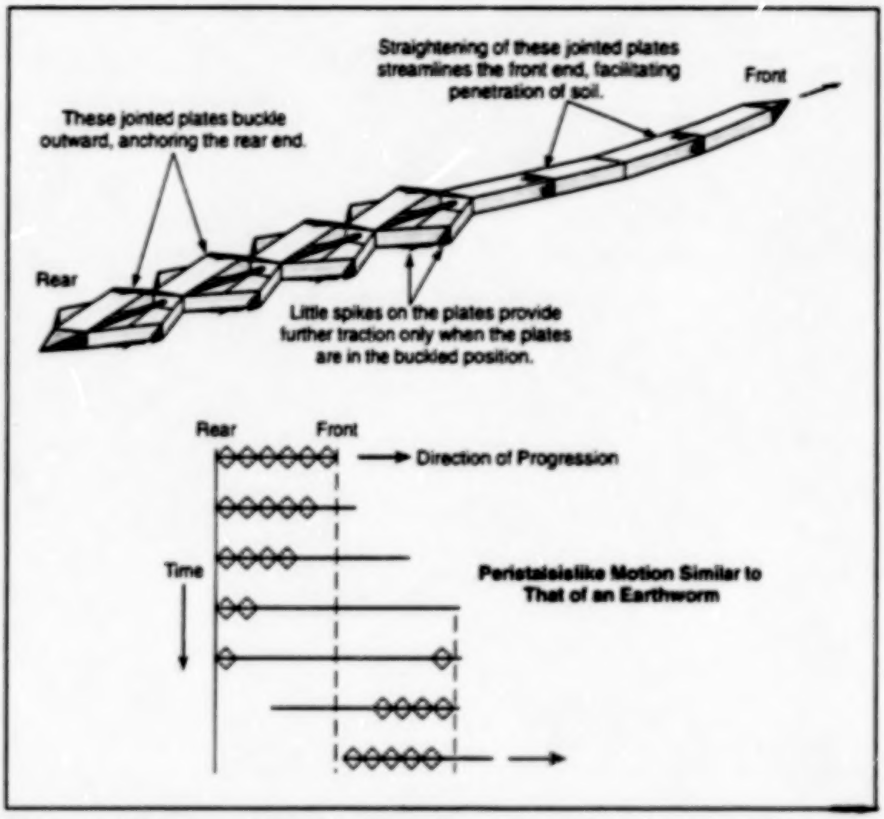

Shortening/Widening and Elongating/Narrowing motions of the segments would be timed to generate an overall peristaltic motion like that of a [illegible]n.

Special-purpose microsensors could be housed in one or more end or middle segment(s). The tips on the end segments could be sharpened to facilitate penetration of soil. Alternatively or in addition, the tips could contain sensors and/or mechanisms to collect samples.

The design of the robot, including the details of the mobility features and the choice of sensors, would be specific to the intended application. For example, an earthwormlike robot might be designed to probe earthquake rubble to find missing persons and animals. The sensors for this application could include a miniature active-pixel-sensor video camera, a temperature sensor, and microspectrometer for detecting carbonates, water, and other chemical signs of life.

This work was done by Sarita Thakoor, Kim Quillin, Alex Fukunaga, John Michael Morookian, and Adrian Stoica of Caltech for **NASA's Jet Propulsion Laboratory**. *Further information is contained in a TSP [see page 1].*
NPO-20266

Miniature Multispeed Transmissions for Small Motors

Transmissions would be batch-fabricated using micromachining technologies.

NASA's Jet Propulsion Laboratory, Pasadena, California

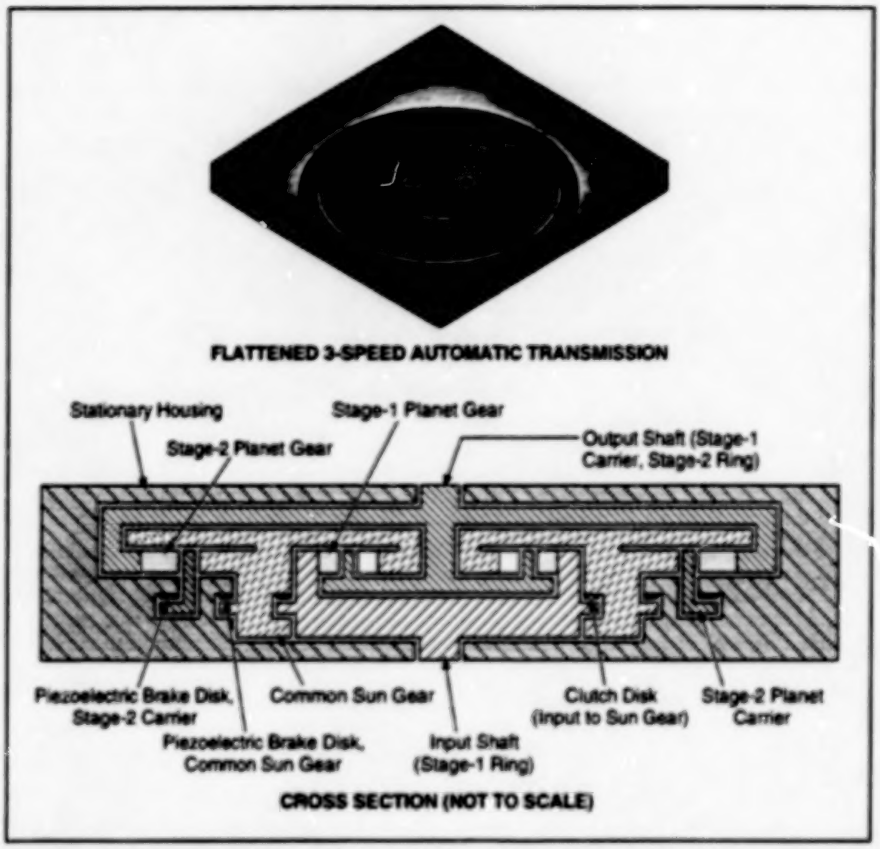

This Miniature Transmission could be regarded as a flattened version of a conventional three-speed automatic transmission. The components would be fabricated by micromachining.

A design has been developed for manufacturing multispeed transmissions that are small enough to be used with minimotors — electromagnetic motors with power ratings of less than 1 W. Like similar, larger systems, such as those in automobiles, the proposed mechanism could be used to satisfy a wider dynamic range than could be achieved with fixed-ratio gearing. However, whereas typical transmission components are machined individually and then assembled, this device would be made using silicon batch-fabrication techniques, similar to those used to manufacture integrated circuits and sensors.

Until now, only fixed-ratio gear trains have been available for minimotors, affording no opportunity to change gears in operation to optimize for varying external conditions, or varying speed, torque, and power requirements. This is because conventional multispeed gear-train geometries and actuation techniques do not lend themselves to cost-effective miniaturization. In recent years, the advent of microelectromechanical systems (MEMS) and of micromachining techniques for making small actuators and gears has created the potential for economical mass production of multispeed transmissions for minimotors. In addition, it should be possible to integrate these mechanisms with sensors, such as tachometers and load cells, as well as circuits, to create integrated silicon systems, which could perform closed-loop speed or torque control under a variety of conditions. In comparison with a conventional motor/transmission assembly, such a package would be smaller and lighter, contain fewer parts, consume less power, and impose less of a computational burden on an external central processing unit (CPU).

Like conventional multispeed transmissions for larger motors, miniature multispeed transmissions would contain gears, clutches, and brakes. However, the designs would be more amenable to micromachining and batch fabrication. Gear stages would be nestled one inside the other (see figure), rather than stacked one over the other, creating a more planar device. Actuators and the housing would be fabricated on separate layers. The complex mechanical linkages and bearings used to shift gears in conventional transmissions would not be practical at the small scales of interest here. Promising alternatives might include electrostatic-friction locks or piezoelectric actuators. For example, in the transmission depicted in the figure, piezoelectric clamps would serve as actuators in clutches and brakes.

The structures would be aligned and bonded, followed by a final etch to release the moving parts. The entire fabrication process can be automated, making it both precise and relatively inexpensive. The end product is a "gearbox on a chip," which can be "dropped" onto a compatible motor to make an integrated drive system.

This work was done by Indrani Chakraborty and Linda Miller of Caltech for **NASA's Jet Propulsion Laboratory**. *Further information is contained in a TSP [see page 1].*

NPO-20316

Improved Hybrid System Protects Airfoils Against Icing

This system includes an upstream thermal and a downstream electromechanical subsystem.

Lewis Research Center, Cleveland, Ohio

An improved hybrid thermal/mechanical system has been developed to protect airplane wings and other airfoils against the accretion of ice, which degrades aerodynamic performance. The system is designed with particular attention to advanced, high-performance airfoils, which exhibit significant loss of lift when their leading edges and adjacent areas become rough, as they do when ice accretes.

In aeronautical terminology, "anti-icing"

denotes the prevention of icing, while "deicing" denotes the removal of ice that has already formed. Anti-icing is the only way to keep the leading edge and adjacent areas of an airfoil aerodynamically smooth in the presence of impinging supercooled water droplets. Deicing is adequate for the area sufficiently downstream of the leading edge, but is not adequate for the leading-edge region because a typical deicing system is not effective until ice has accreted to some minimum thickness, and some residual ice sometimes remains after a deicing cycle.

In the most common approach to anti-icing, one heats the leading edge and adjacent roughness-sensitive area to evaporate the impinging supercooled droplets when flying through a cloud. However, the power demand of a fully evaporative anti-icing system is excessive for most light jet and regional turboprop airplanes. The present hybrid system was developed to enable the anti-icing and deicing of such airplanes at an acceptably low power demand.

This hybrid system includes an upstream thermal anti-icing subsystem, a downstream electromechanical deicing subsystem (see figure), and an electronic subsystem that controls the other two subsystems. The thermal subsystem heats (either electrically or by use of hot gas from the engine) the leading-edge region enough to prevent water from freezing, but not enough to evaporate most of the water. No such heating is performed in the area downstream of the leading-edge region for the following reasons: Water from the leading-edge region runs back along the surface in rivulets, so that most of the downstream area is dry most of the time. As a result, heating most or all of the downstream area in order to heat the wet spots would be inefficient, entailing excessive power demand.

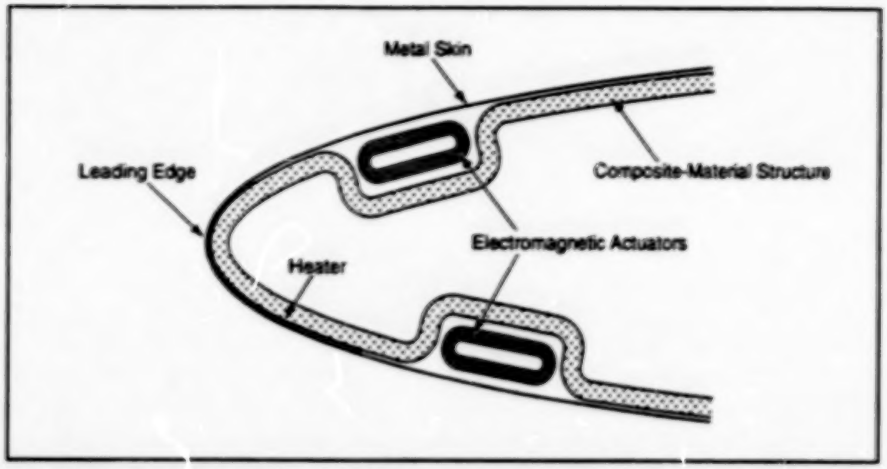

The Heater Prevents Freezing of impinging supercooled water droplets in the leading-edge region. The electromagnetic actuators occasionally deflect the metal skin outward to knock off ice that accumulates downstream from the leading edge.

The electromechanical deicing subsystem includes actuators inside the airfoil at downstream locations on the upper and lower airfoil surfaces. These are locations where ice forms by freezing of impinging droplets and of water that runs back from the leading edge. The actuators are basically electromagnetic coils to which large dc pulses are occasionally applied, as required, by discharging energy-storage capacitors, creating a rapid impulsive force. The electromagnetic force causes the actuators to expand perpendicularly to the skin. The airfoil skin momentarily deflects very slightly outward, with high level of acceleration, and returns to its original position. This is the actuation that removes the accumulated ice. Although the momentary pulse power is high, the average power consumed by the electromechanical subsystem is low.

This work was done by Kamel Al-Khalil, Dennis Phillips, and Thomas Ferguson of Cox & Co., Inc., for **Lewis Research Center.** *Further information is contained in a TSP [see page 1].*

Inquiries concerning rights for the commercial use of this invention should be addressed to NASA Lewis Research Center, Commercial Technology Office, Attn: Tech Brief Patent Status, Mail Stop 7–3, 21000 Brookpark Road, Cleveland, Ohio 44135. Refer to LEW-16412.

A Technique for Compensating Joint Limits in a Robot Manipulator

Upon saturation of a joint, control demand is redistributed among remaining unsaturated joints.

Lewis Research Center, Cleveland, Ohio

A robust, optimal, adaptive technique for compensating rate and position limits in the joints of a six-degree-of-freedom manipulator has been developed. In this new algorithm, the unmet demand as a result of actuator saturation is redistributed among the remaining unsaturated joints. The scheme is used to compensate for inadequate path planning, problems such as joint limiting, joint freezing, or even obstacle avoidance, where a desired position and orientation are not attainable due to an unrealizable joint command. Once a joint encounters a limit, supplemental commands are sent to other joints to

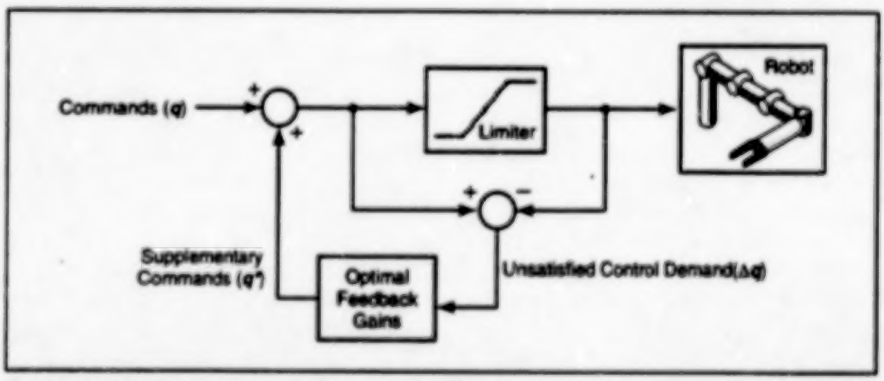

Robot Joint Commands are used with optimal joint limit compensation. The unmet demand, which would otherwise saturate a joint, is fed back through the optimal gains to provide supplemental commands to joints with authority remaining.

best track, according to a selected criterion, the desired trajectory.

A standard six-degree-of-freedom manipulator has six independently controlled joints. The position and orientation of the end effector, each of which is described in three dimensions, are fully determined by the angles of the joints. As long as the appropriate joint angles are achievable, the desired position and orientation can be obtained. However, when the specified joint trajectories cannot be followed due to a command beyond the range of the actuator, positions and orientations downstream from the limited joint will all be affected, causing in some cases extreme deviations from the expected values. This new scheme is an ideal solution candidate for this problem. It was designed to compensate for actuator saturation in a multivariable system by supplementing the commands to the remaining actuators to produce the desired effect on the output, in this case the gripper position and orientation. For each joint which saturates, a degree of freedom is lost, but the remaining joints can be used to track the desired path within the physical limits of the manipulator.

The matrix known as the Jacobian, J, describes how a small change in the joint positions, dq, affects the gripper. The resulting position and orientation change of the end effector, D, is computed as $D = Jdq$. When a joint is commanded to move beyond its limit, a portion of the command cannot be achieved. This unmet demand, Δq, represents the amount the joints should move but cannot. The resulting error in position and orientation of the end effector can be approximated by $D=J\Delta q$. The objective of this new scheme is to duplicate D as closely as possible using joints with authority remaining.

The figure shows the scheme with the optimal gains in the feedback loop. The commands, q, are checked to verify that they will not drive any of the joints to a rate or position limit. Any portion of a command which would cause a joint to saturate corresponds to unmet demand and is truncated and redirected to the feedback gains. The gains take this unmet demand, Δq, and produce some supplemental commands to unsaturated joints, q^*, such that $J\Delta q$ and $J\,q^*$ are as close as possible. These supplemental commands allow the end effector to optimally track its desired trajectory, even in the face of joint position and rate limits. Since the algorithm acts upon the joint commands only, there is never the possibility of an unstable system resulting from the use of this algorithm.

The optimal feedback gains are computed using a quadratic objective function with task-dependent weights assigned to the components of the position and orientation vector of the end effector. The gains adapt to changes in the Jacobian as the manipulator moves through its workspace, and the computations are robust to singularities arising from particular manipulator configurations. This provides smooth, continuous variation of the optimal gains for as long as Δq is nonzero.

This work was done by Ten-Huei Guo of **Lewis Research Center**, *Jonathan Litt of the Vehicle Technology Center of the U.S. Army Research Laboratory, and André Hickman of Morehouse College. Further information is contained in a TSP [see page 1].*

Inquiries concerning rights for the commercial use of this invention should be addressed to NASA Lewis Research Center, Commercial Technology Office, Attn: Tech Brief Patent Status, Mail Stop 7-3, 21000 Brookpark Road, Cleveland, Ohio 44135. Refer to LEW-16566.

Pulse-tube Refrigerator Unit

The working fluid for this new device is helium, which is nontoxic to humans and harmless to the environment.

Marshall Space Flight Center, Alabama

The Pulse-tube Refrigeration unit offers a viable alternative to units that currently require chlorofluorocarbon (CFC) and hydro-chlorofluorocarbon (HCFC) working fluid. Pulse-tube Refrigerators use helium as the working fluid, which is nontoxic to humans and harmless to the environment.

Pulse-tube Refrigerators can be operated over a wide range of temperatures. These units can be used in numerous space and commercial refrigeration applications, including food refrigerator/freezers, laboratory freezers, and freeze dryers. Pulse-tube Refrigerators can also be used to cool detectors and electronic devices.

Pulse-tube Refrigeration, a variation of the Stirling cycle, is a relative newcomer compared to other refrigeration cycles.

The Pulse-tube Refrigerator is the first unit applied to the temperature range and load level needed for typical food freezers and laboratory freezers.

The design of the Pulse-tube Refrigerator unit was based on the Orifice Pulse-tube concept. First, the gas is compressed in the compressor. Next, it flows through the compressor aftercooler, where heat is rejected to a water-cooling loop. Then the gas flows through the regenerator, which is basically an economizer, conserving cooling from one cycle to the next. The gas then enters the cold-end heat exchanger where heat is added to the gas from the surroundings.

The gas finally enters the Pulse Tube, orifice, and reservoir. These three components produce the phase shift of the mass flow and pressure, which is necessary for cooling. The gas shuttles back and forth between the hot and cold ends rather than circulating continuously around a loop, as in some refrigeration cycles. Heat is lifted against the temperature gradient and rejected at the hot-end heat exchanger, which is also water-cooled.

The compressor designed and built for this unit is a dual-opposed-piston type. The displacement of these two pistons is 180° out of phase, to reduce vibrations. The compressor, which can be operated over a wide range of frequencies, is designed for operation at a nominal 60 Hz.

The compressor pistons are supported by helical mechanical springs which assist in producing harmonic motion and return the pistons to the needed null positions before startup. The pistons are supported inside the cylinders on dry lubricated, low-friction sleeve bearings. Each piston is attached to a separate moving coil, which is formed by wrapping copper wire around the end of a spool. When voltage is applied to a coil, the resulting current produces a force on the coil.

Optical encoders provide real-time readout of all piston positions. These encoders use a noncontacting interrupter scale between a light-emitting-diode source and sensors to detect motion. A tachometer pulse and direction signal are generated.

The cold-end and hot-end heat exchangers consist of fine mesh copper screens, fabricated in-house using proprietary techniques.

After design and fabrication, the Pulse-tube Refrigerator unit was subjected to

numerous tests. A temperature of –45 °C was reached, which is well below the temperature required for food freezers.

Pulse-tube Refrigerators offer increased reliability, fewer moving parts, and much lower cold-end vibration than other spacecraft or commercial refrigeration concepts.

This work was done by W.G. Dean of Dean Applied Technology Co. for **Marshall Space Flight Center**. *Further information is contained in a TSP [see page 1].*

In accordance with Public Law 96-517, the contractor has elected to retain title to this invention. Inquiries concerning rights for its commercial use should be addressed to:

Dean Applied Technology, Inc.
1580 Sparkman Drive #103
Huntsville, AL 35816
(205) 721-9550

Refer to MFS-26440, volume and number of this NASA Tech Briefs *issue, and the page number.*

Hydraulically Driven High-Speed Spindle for General Machining

Improved design for high-speed spindles increases strength and rigidity and improves balance.

Marshall Space Flight Center, Alabama

A hydraulically driven high-speed spindle system for milling, machining, facing, drilling, and joining metallic and nonmetallic materials has been developed. Spindles are the most critical elements of high-speed milling machines. The keys to successful design of high-speed spindles are strength, rigidity, and balance.

The hydraulically driven spindle includes a hydraulically driven gearmotor. The rotation of the motor is transmitted to the main shaft of the spindle. The main shaft supports a fixture that holds the tool to effect the desired operation. The main shaft is supported by a series of bearings that withstand axial and radial loads encountered during use. The pressure and flow rate can be adjusted manually or controlled by a computer. This system includes a hydraulic subsystem that supplies pressurized fluid to drive the spindle.

Pressurized fluid is fed into the hydraulically driven spindle for machining, milling, drilling, tapping, facing, and joining. Hydraulic fluid volumetric flow rate, fluid pressure, gear size, and geometry of the hydraulic motor are variables which govern spindle torque and rotational speed, ranging from 5,000 to 6,000 rpm and operating at 1,000- to 6,000-psi (6.9- to 4-MPa) pressures.

The bearing system for this hydraulically driven spindle can be made of recently developed fluid bearings or of roller element type bearings. The balls in the bearings in this system can be made of standard steel or of newly-developed ceramics for increased rigidity, accuracy, and longer life. Bearings that are designed for use at lower speeds with air/oil or air/mist lubrication can be used at higher speeds, provided they are lubricated with grease.

High-speed machining allows for the production of thin wall sections with minimal deformation. High-speed machining can make it possible to reduce the number of parts, sometimes even making it possible to fabricate, as unitary parts, objects that would ordinarily have to be assembled from multiple pieces. Therefore, production and assembly times are reduced.

For the purpose of fabricating complex and thin-walled parts, high-speed machining of solid stock can be an alternative to casting and to the more expensive use of composite materials. Use of this hydraulically driven spindle system for high-speed machining reduces times and cost of the manufacturing process and helps to ensure defect-free finished parts.

Another significant advantage of high-speed machining is minimization of effects of heat on machined parts. Most of the cutting heat is removed, reducing thermal warping and increasing the life of the cutting tool. In many cases, the need for a cooling fluid is eliminated. Also, elimination of cutting fluids reduces subsequent contributions to pollution and aids in the recovery and recycling of such expensive materials as aluminum-lithium alloys.

This work was done by Majid K. Babai and Samuel C. Geise of **Marshall Space Flight Center**. *Further information is contained in a TSP [see page 1].*

Inquiries concerning rights for the commercial use of this invention should be addressed to the Patent Counsel, Marshall Space Flight Center [see page 1].

Refer to MFS-26430.

Books and Reports

Hybrid Propulsion System for Returning a Sample From Mars

A paper suggests the development of a hybrid rocket engine and associated equipment for returning a sample of material from Mars at relatively low cost. In a hybrid rocket engine, a solid fuel is burned by use of a liquid or gaseous oxidizer, the flow of which can be throttled to control the engine. Unlike conventional solid rocket propellants, a solid rocket fuel can be made relatively inert in the absence of the oxidizer and therefore presents little hazard of explosion or inadvertent ignition. Unlike conventional (and relatively expensive) liquid rocket propellants, a solid rocket fuel is not corrosive or susceptible to leakage. The solid fuel in the proposed system would be in granular form, packed into the rocket motor. Oxygen or another suitable oxidizer could be transported from Earth together with this solid fuel. Alternatively, oxygen could be generated from CO_2 in the Martian atmosphere by use of in-situ resource utilization (ISRU) equipment. Inasmuch as ISRU is not yet a mature technological discipline, some research on ISRU would be necessary to estimate the reduction in cost achieved by not having to carry the oxidizer to Mars.

This work was done by Kumar Ramohalli of Caltech for **NASA's Jet Propulsion Laboratory**. *To obtain a copy of the paper, "Hybrids for Low-Cost Sample Return Missions," see TSP's [page 1].*

NPO-20195

BLANK PAGE

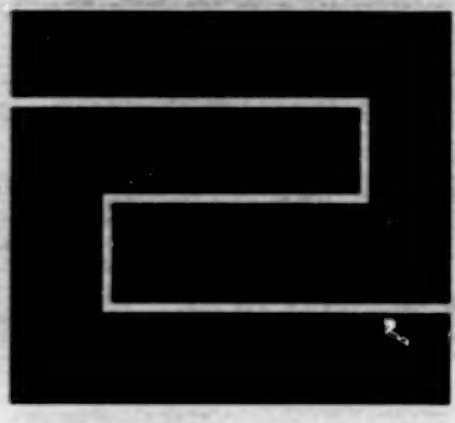

Fabrication Technology

Hardware, Techniques, and Processes

BLANK PAGE

Apparatus for Coating and Cold Welding in Vacuum

Vacuum need not be broken between the coating and cold-welding processes.

Lewis Research Center, Cleveland, Ohio

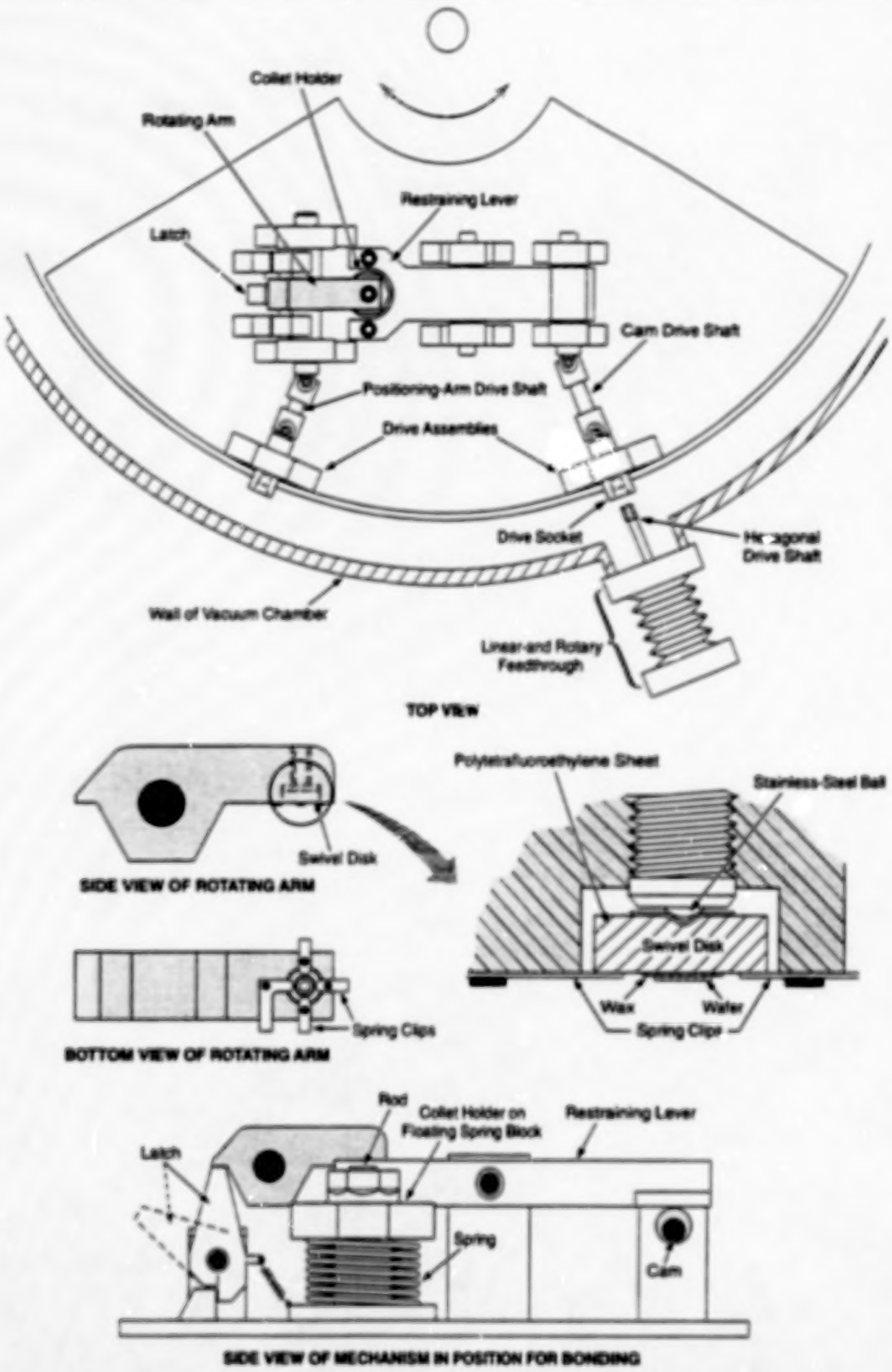

The **Wafer Can Be Positioned** facing upward toward a metal-deposition source, the turntable can be turned to bring the rod and disk to different metal-deposition sources, and the metal-coated wafer can be pushed down onto the rod for cold welding, all without breaking vacuum.

The figure illustrates selected aspects of a manually actuated apparatus for use in coating two small objects with suitable metals, then forcing the two objects together at the coated flat surfaces with uniform pressure to cold-weld them to each other. The design of this apparatus provides for all steps of the coating and cold-welding processes, including intermediate steps of manipulation between these processes, to be performed in a vacuum, with no need to break vacuum between the processes as in older methods of coating and cold welding. By maintaining vacuum through all processing steps, one prevents the formation of surface oxides, which interfere with cold welding. Maintaining vacuum also prevents the formation of pockets of trapped gas, which render the bond nonuniform.

In the original application for which the apparatus was designed, the objects to be joined are components of an ultrasonic transducer; namely, a piezoelectric (e.g., lithium niobate) wafer as thin as 0.001 in. (25 μm) and a round sapphire rod with a flat surface (to mate with the wafer) at one end and a concave focusing surface at the other end. The faying surfaces of the rod and disk must be coated with thin layers of chromium, then gold, then indium, by sputtering or vapor deposition in a vacuum. Then the wafer is pressed onto the end of the rod with a pressure of about 300 kg/cm^2 (about 0.1 MPa) to cold-weld the rod and disk together at the indium surface layers. Thinness and uniformity of the bond layers and uniformity of the cold-weld joint are necessary for proper acoustic performance.

The apparatus includes a collet that holds the sapphire rod and a rotating arm that contains a swivel disk, on which the wafer is held by a layer of wax. The arm enables the initial pickup of the prealigned wafer, the orientation of the wafer facing a metal-deposition source, and the repositioning of the wafer for subsequent bonding to the rod. During coating with metal, both the rod and the wafer are oriented with the bonding surfaces to be coated facing the source of the metal. The chromium, gold, and indium layers are deposited from three different sources. The apparatus includes a turntable so that the rod and wafer can be positioned below each of the three sources in sequence.

The collet is mounted in a spring-loaded holder, the springs of which are preadjusted to provide the appropriate bonding force. The springs are compressed and restrained by a cam-actuated lever. The cam is driven by a linear-and-rotary vacuum feedthrough that enables actuation without breaking vacuum. The feedthrough can be made to engage a cam socket when the angular position of the rotary table is such that the cam socket and the feedthrough are aligned with each other.

A similar feedthrough and cam-actuation mechanism is provided for the positioning arm. The arm is initially set in the coating position. After deposition of the three metal layers, the arm is rotated, by use of this mechanism, to push the wafer down onto the rod in the collet. The swivel disk provides limited freedom of tilt to allow the wafer to align itself with the tip of the rod when the wafer and rod are pushed together. A latch locks the arm into position for bonding. A restraining cam is rotated to unload the spring compression from a restraining lever, allowing the spring to press the wafer and rod together.

After the pressing, the vacuum system can be opened. Spring clips that hold the swivel disk in place and the collet that holds the rod in place are loosened, making it possible to remove the bonded parts with the swivel disk still attached to the wafer by wax. The swivel disk is released by gently heating the parts to melt the wax.

This work was done by Richard Oeftering and Floyd Smith of **Lewis Research Center**. *Further information is contained in a TSP [see page 1].*

Inquiries concerning rights for the commercial use of this invention should be addressed to the Patent Counsel, Lewis Research Center [see page 1]. Refer to LEW-15922.

Device for High-Pressure Fused Deposition of Engineering Polymers From Feed Rods

New technology builds a solid object from true functional engineering materials.

Marshall Space Flight Center, Alabama

A more versatile delivery system for fused deposition has recently been developed. This system uses a very stiff, precise, and compact actuator to drive a small piston/cylinder extruder that has a heated nozzle. Because feed rods are used as the feed material, this newly developed delivery system does not have the materials limitations of conventional delivery systems.

This innovative technology is a mechanical assembly that can achieve high extrusion pressure that can be constructed in a compact enough form to retrofit existing fused deposition systems. The heart of this mechanical system is the combination of a hollow cylindrical servo motor and a ball screw, which are used to directly drive the piston of a piston extruder. The end of the screw is secured on a plate, which slides on four posts to provide counterrotation. This plate also prevents any axial misalignment of the screw and houses the load cell. The four posts provide a frame that attaches to a top plate to support the motor and a bottom plate to support the cylinder of the piston extruder. These elements form a very stiff mechanical linkage with very low lag or backlash and produce very precise volumetric displacement of material.

A completed ACR in-house **High-Pressure Fused-Deposition System** is depicted in this photo.

The cylindrical pancake motors for this invention were designed to eliminate gear reductions and avoid backlash in direct-drive equipment. Because the stator has been moved to the outside of the rotor, these motors produce very high torque at

extremely low and controlled angular velocities. The increased radius and mass of the rotor translate to very high torque and rotor inertia. Also, the cylindrical motor is hollow, which allows the ball nut to fit inside the motor. This makes the actuator assembly very compact.

Two configurations of the high-pressure deposition were fabricated. One configuration was designed to retrofit into a Statasys Fused Deposition Modeler (FDM). The second configuration was designed for an Advanced Ceramics Research, Inc., (ACR) in-house fused deposition system. In the FDM, the head is moved in the horizontal plane and material is deposited onto a base that is moved vertically. In the ACR in-house system, the head is mounted on a stationary bridge and material is deposited onto a base which is moved in the horizontal plane and vertically beneath the head. The ACR system has more piston displacement, but the basic design of both units is the same.

This innovative technology has been used to free-form a number of important functional materials, such as polyaryletherketone, polycarbonate, thermoplastic polyurethane, and polylactic acid/poly-glycolic acid block copolymer. This delivery system has also been used to fabricate green bodies that were subsequently fired to high density, including alumina, yttria stabilized zirconia, and silicon nitride.

Testing of these materials showed that the mechanical properties of the materials systems developed with this new invention greatly surpassed those of other free-formed polymer materials.

This work was done by Peter Creegan, Robert Hoffman, and Gabriel Chambers of Advanced Ceramics Research, Inc., and Kevin Stuffle of Materials and Machines, Inc., for **Marshall Space Flight Center**. *Further information is contained in a TSP [see page 1].*

Inquiries concerning rights for the commercial use of this invention should be addressed to the Patent Counsel, Marshall Space Flight Center [see page 1]. Refer to MFS-26446.

BLANK PAGE

Mathematics and Information Sciences

Hardware, Techniques, and Processes

BLANK PAGE

Wavelet Processing for Aeroservoelastic-Stability Analysis

Stability margins are more realistic and robust than those obtained by older techniques.

Dryden Flight Research Center, Edwards, California

A wavelet-based modal-parameter-extraction procedure has been developed to augment wavelet filtering and thereby produce more-realistic, robust aeroservoelastic-stability margins. The procedure is intended for use in processing data from aircraft flight tests.

Some background information is prerequisite to an explanation of this development. Deterministic nonstationary input test signals are often essential for extracting aeroelastic-stability trends from noisy measurements. The analysis of flight data is improved by discrimination among areas of low signal-to-noise ratio, unmodeled dynamics, and external disturbances. Wavelet signal processing has shown promise for identification of the conceptual structures, operators, and parameters of mathematical models (hereafter called "system identification") of aeroservoelastic systems for these purposes.

Nonparametric wavelet filtering removes aspects of signal responses detrimental to linear system-identification methods to improve stability tracking. Wavelet transforms are also used to directly supply information on time-dependent modal decay rates and phases for estimation of parameters of mathematical models of time-varying systems. Without any approximation of the range of parameters of a system, natural frequencies and damping ratios are extracted from the response of the system. Damping and frequency trends are useful for noting changes in system dynamics as functions of flight conditions.

Model validation is a critical procedure in the computation of robust stability margins. The margins are adversely affected by poor characterizations of uncertainty size and structure, which are determined by the magnitudes of perturbations, locations of perturbations within the system, and the types (real or complex) of perturbations. This completes the background information.

In the present wavelet-based modal-parameter-extraction procedure, both complex, nonparametric and real, parametric perturbations are decreased to generate reduced-norm uncertainty sets, which result in models with less conservatism. The models are used in a robust stability-boundary-prediction method called the "μ method" because it is based on a structured singular value called "μ." [This method was described in "Characterizing Worst-Case Flutter Margins From Flight Data" (DRC-97-03), *NASA Tech Briefs*, Vol. 21, No. 4 (April 1997), page 62.]

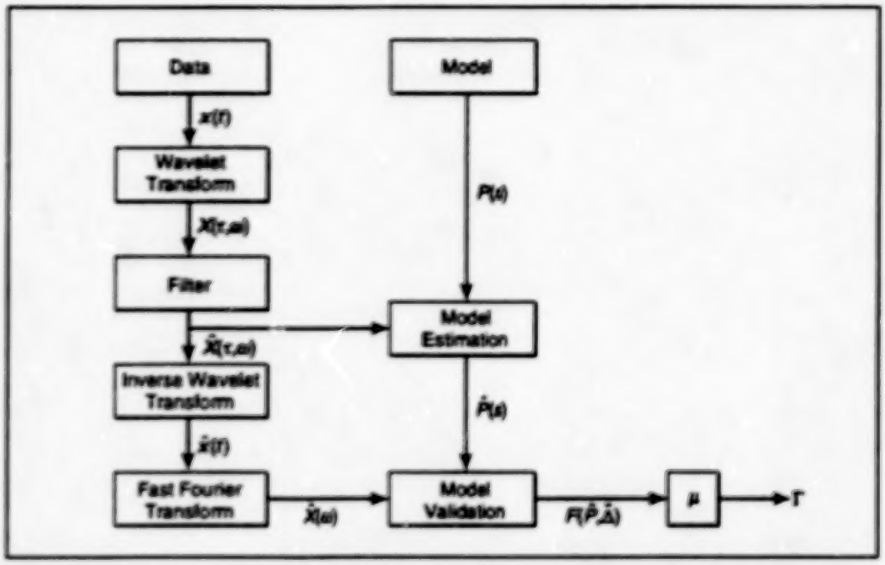

The Flows of Information represented graphically here are those that occur when the μ method is coupled with wavelet processing for robust stability-margin analysis of an aeroservoelastic system.

Within the μ conceptual framework, a system is represented as an operator, $F(P,\Delta)$, which, in turn, represents a feedback interconnection of a plant P and uncertainty Δ. Flight data can be incorporated into the μ method by formulating a description of uncertainty that accounts for observed variations and errors. A model-validation analysis is performed on the plant model to ensure that the range of dynamics admitted by the uncertainty is sufficient to cover the range of dynamics observed with the flight data.

The μ method can be coupled with wavelet processing for parametric and nonparametric estimation. This coupling is achieved by introducing, into the basic process, several time-frequency operations based on wavelet filtering (see figure). Wavelet transform operations are introduced to process time-domain data, $x(t)$, before computation of a frequency-domain representation, $\hat{X}(\omega)$. These operations map the time-domain data into the time-frequency domain via a wavelet transform, then map them back to the time domain via an inverse wavelet transform. A time-frequency filtering operation is performed between the wavelet transform and the inverse wavelet transform to remove unwanted features before the inverse wavelet transform yields a time-domain signal, $\hat{x}(t)$.

A modal-parameter-estimation algorithm is introduced by use of the wavelet algorithm. The estimated parameters are used to update the elements of a nominal plant model, P, and a new plant model, $\hat{P}$, is used to represent the dynamics of the aeroservoelastic system.

The final operations of the μ method are traditional robust-stability operations on frequency-domain data. The effect of the wavelet filtering is to introduce filtered versions of the data and the plant model for model validation. Thus, a new uncertainty operator, $\hat{\Delta}$, is associated with the parameter-updated plant, $\hat{P}$, to account for errors observed from the filtered data, $\hat{x}(t)$. There is computed a robust stability margin, Γ, that describes the largest change in dynamic pressure for which $\hat{P}$ is robustly stable to the errors, $\hat{\Delta}$.

Nominal stability margins are computed for the plant model by use of the original theoretical modal parameters and are computed for the updated model by use of parameters estimated from wavelet filtering. These margins are computed from a μ analysis with respect to variation in dynamic pressure, $\bar{q}$, but ignoring the modal and complex uncertainty operators.

This work was done by Martin J. Brenner of **Dryden Flight Research Center** *and Rick Lind of NRC. Further information is contained in a TSP [see page 1].*

DRC-98-26

Automated System for Acting on Findings From Inspections

Real-time access by all concerned parties fosters understanding of the condition of hardware.

Stennis Space Center, Mississippi

This Interactive Display is one in a sequence of such displays presented to the user for entry of data into an IDCR.

The Automated Nonconformance System, based at Stennis Space Center, is a computer network dedicated to administration of inspections and repairs of rocket engines. This automated system was developed to replace a manual system in which paper documents were used to document the steps of inspection and repair processes, and in which the documents had to be handled and transferred repeatedly according to complex procedures designed to ensure the completion of interdependent process steps in the correct sequences.

The basic paper document in the manual system — called the "Inspection Discrepancy and Correction Record" (IDCR) — has been converted into a collection of menu-driven interactive alphanumerical and graphical computer displays (see figure) in the automated system. It is still necessary to follow the complex procedures, but the automated system eliminates the paperwork delays and the potential for paperwork error, and enables all interested parties at diverse locations to gain access to inspection and repair data in real time. In so doing, the automated system fosters a high degree of awareness of the condition of the inspected and repaired hardware and helps to ensure that all technical and organizational requirements are satisfied.

The automated system affords capabilities to generate IDCRs, to import photographs and drawings from previous inspection and repair processes, to apply and void the electronic equivalent of stamps that were previously applied to paper to document authority to perform or authorize various process steps, to identify required process steps that have not yet been completed, and to perform numerous other functions essential to documenting inspection and repair processes. Passwords are used to control access to the system, and as evidence of authority to apply and void stamps. The automated system also performs audits to prevent both (1) duplication of work and (2) shipping out a piece of hardware before all required process steps have been performed, all necessary stamps applied, and all documentation completed.

This work was done by Victor O. Alfaro, Sr., and Robert M. Robb of Boeing, Rocketdyne Propulsion & Power for **Stennis Space Center.** *Further information is contained in a TSP [see page 1].*
SSC-00054

Computer Network for Management of Inspection Data

Users need not travel to view original inspection records and archival documents.

Stennis Space Center, Mississippi

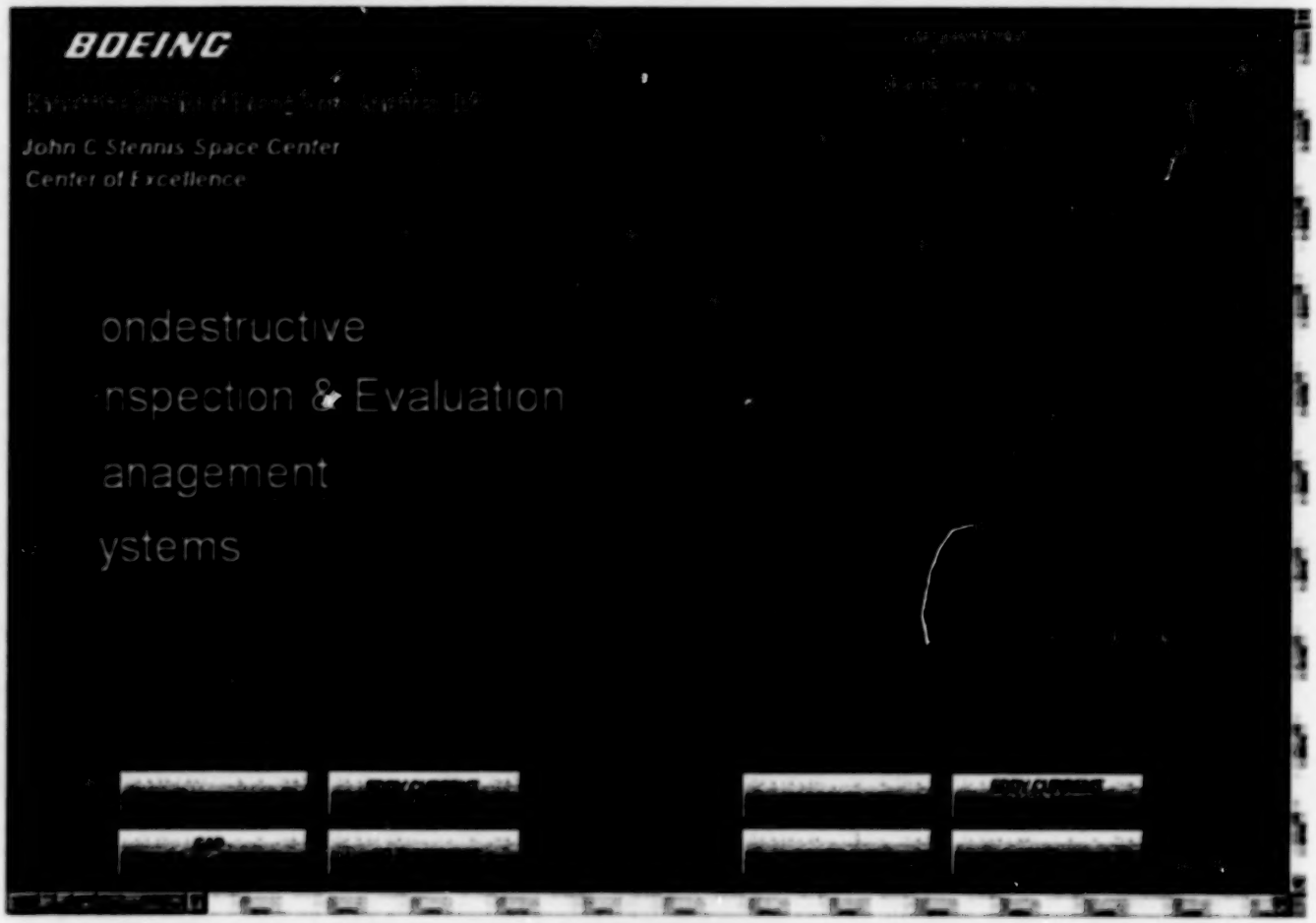

Computer Displays With Full Graphical Capabilities enable individuals at various locations to view inspection records.

The *Nondestructive Inspection and Evaluation Management System* (NIMS), based at Stennis Space Center, is a computer network dedicated to administration of a large data base pertaining to nondestructive inspections of rocket-engine components. The NIMS serves as both an electronic archive of inspection records and as a communication medium. Inspection records can be in a variety of forms, include ordinary photographs, fluorescent-penetrant images of cracks, eddy-current traces, images from ultrasonic scans, and sketches.

One important benefit afforded by the NIMS is providing rapid, easy access to records of previous inspections. Inspectors and engineers often need to view such records to obtain guidance in the interpretation of records of new inspections and in the development of new inspection techniques. Before the development of the NIMS, it was necessary to engage in a labor-intensive and time-consuming procedure of retrieving original inspection records from archives, photocopying them, and sending the photocopies to the requesting engineers and inspectors.

Another important benefit afforded by NIMS is enabling a person at one location to view, in real time, the record of an inspection performed by another person at a different location, in order to discuss or confirm the interpretation of the record. Before the development of the NIMS, it was common practice to transmit copies of the inspection records by facsimile ("fax") for this purpose, but the degradation of image quality by facsimile transmission often rendered the copies useless, making it necessary for the assisting engineer and inspectors to travel to the inspection sites. With the NIMS, one can view a photographic-quality copy of an inspection record from any location in the network.

The NIMS is compatible with IBM and Macintosh, or compatible, computers. It accommodates new inspection records and new types of inspections as needed, without extensive programming changes. Security is maintained by requiring passwords for access by users and guests.

This work was done by Victor O. Alfaro, Sr., Robert M. Robb, and Michael F. Reynolds of Boeing, Rocketdyne Propulsion & Power for **Stennis Space Center.** *Further information is contained in a TSP [see page 1].*

SSC-00055

National Aeronautics and
Space Administration

64

END

10\08\98